



This is a repository copy of *Enlargement of ribbons in zebrafish hair cells increases calcium currents, but disrupts afferent spontaneous activity and timing of stimulus onset.*

White Rose Research Online URL for this paper:
<http://eprints.whiterose.ac.uk/117035/>

Version: Accepted Version

Article:

Sheets, L., He, X.J., Olt, J. et al. (9 more authors) (2017) Enlargement of ribbons in zebrafish hair cells increases calcium currents, but disrupts afferent spontaneous activity and timing of stimulus onset. *Journal of Neuroscience*. ISSN 0270-6474

<https://doi.org/10.1523/JNEUROSCI.2878-16.2017>

Reuse

This article is distributed under the terms of the Creative Commons Attribution (CC BY) licence. This licence allows you to distribute, remix, tweak, and build upon the work, even commercially, as long as you credit the authors for the original work. More information and the full terms of the licence here:
<https://creativecommons.org/licenses/>

Takedown

If you consider content in White Rose Research Online to be in breach of UK law, please notify us by emailing eprints@whiterose.ac.uk including the URL of the record and the reason for the withdrawal request.



eprints@whiterose.ac.uk
<https://eprints.whiterose.ac.uk/>

Research Articles: Cellular/Molecular

Enlargement of ribbons in zebrafish hair cells increases calcium currents, but disrupts afferent spontaneous activity and timing of stimulus onset

Lavinia Sheets^{2,3}, Xinyi J. He¹, Jennifer Olt⁶, Mary Schreck¹, Ronald S. Petralia⁷, Ya-Xian Wang⁷, Qiuxiang Zhang¹, Alisha Beirl¹, Teresa Nicolson⁵, Walter Marcotti⁶, Josef G. Trapani⁴ and Katie S. Kindt¹

¹Section on Sensory Cell Development and Function, NIDCD/National Institutes of Health, Bethesda, MD 20892 USA

²Department of Otolaryngology, Harvard Medical School, Boston, MA 02115 USA

³Eaton -Peabody Laboratory, Massachusetts Eye and Ear, Boston, MA 02114 USA

⁴Department of Biology and Neuroscience Program, Amherst College, Amherst, MA 01002 USA

⁵Oregon Hearing Research Center and Vollum Institute, Oregon Health & Science University, Portland, OR 97239 USA

⁶Department of Biomedical Science, University of Sheffield, Sheffield, United Kingdom

⁷Advanced Imaging Core, NIDCD/National Institutes of Health, Bethesda, MD 20892, USA

DOI: 10.1523/JNEUROSCI.2878-16.2017

Received: 13 September 2016

Revised: 26 April 2017

Accepted: 27 April 2017

Published: 25 May 2017

Author contributions: L.S., J.O., J.G.T., W.M., T.N., and K.K. designed research; L.S., X.J.H., J.O., J.G.T., M.S., K.K., q.Z., A.B., R.S.P., and Y.-X.W. performed research; L.S., X.J.H., J.O., J.G.T., M.S., K.K., and q.Z. analyzed data; L.S., J.G.T., and K.K. wrote the paper.

Conflict of Interest: The authors declare no competing financial interests.

This study was supported by National Institutes of Health Grants R01 DC006880 (T.N.), P30 DC005983 (PI: Peter Barr-Gillespie), and R15 DC014843 (J.G.T.), the Howard Hughes Medical Institute (T.N.), the Amelia Peabody Charitable Fund (L.S.), NIH/NIDCD intramural research funds 1ZIADC000085-01 (K.S.K.), and ZICDC000081 (R.S.P. and Y.W.), and a Wellcome Trust grant 102892 (W.M.). We would like to acknowledge Catherine Weisz, Katie Drerup, and Cole Graydon for their thoughtful comments on the manuscript.

Corresponding author: Katie Kindt: katie.kindt@nih.gov

Cite as: J. Neurosci ; 10.1523/JNEUROSCI.2878-16.2017

Alerts: Sign up at www.jneurosci.org/cgi/alerts to receive customized email alerts when the fully formatted version of this article is published.

This is an open-access article distributed under the terms of the Creative Commons Attribution 4.0 International license, which permits unrestricted use, distribution and reproduction in any medium provided that the original work is properly attributed.

Accepted manuscripts are peer-reviewed but have not been through the copyediting, formatting, or proofreading process.

1 Title: Enlargement of ribbons in zebrafish hair cells increases calcium currents, but disrupts
2 afferent spontaneous activity and timing of stimulus onset

3 **Abbreviated title:** Relating hair-cell ribbon size to function

4 **Authors:** Lavinia Sheets^{2,3}, Xinyi J. He¹, Jennifer Olt⁶, Mary Schreck¹, Ronald S. Petralia⁷, Ya-Xian
5 Wang⁷, Qiuxiang Zhang¹, Alisha Beir¹, Teresa Nicolson⁵, Walter Marcotti⁶, Josef G. Trapani⁴ and
6 Katie S. Kindt^{1*}

7
8 ¹Section on Sensory Cell Development and Function
9 NIDCD/National Institutes of Health
10 Bethesda, MD 20892 USA

11
12 ²Department of Otolaryngology
13 Harvard Medical School
14 Boston, MA 02115 USA

15
16 ³Eaton -Peabody Laboratory
17 Massachusetts Eye and Ear
18 Boston, MA 02114 USA

19
20 ⁴Department of Biology and Neuroscience Program
21 Amherst College
22 Amherst, MA 01002 USA

23
24 ⁵Oregon Hearing Research Center and Vollum Institute
25 Oregon Health & Science University
26 Portland, OR 97239 USA

27
28 ⁶Department of Biomedical Science,
29 University of Sheffield, Sheffield,
30 United Kingdom

31
32 ⁷Advanced Imaging Core
33 NIDCD/National Institutes of Health
34 Bethesda, MD 20892, USA

35
36
37 *** Corresponding author**
38 Katie Kindt: katie.kindt@nih.gov

39
40 **Number of pages:** (46)

41 **Number of:** Figures (7) Tables (0) multimedia and 3D models (0)

42 **Number of words:** Abstract (191) Introduction (668) Discussion (1476)

43

44 **Conflict of Interest:** The authors declare no competing financial interests.

45 **Acknowledgements:** This study was supported by National Institutes of Health Grants R01
46 DC006880 (T.N.), P30 DC005983 (PI: Peter Barr-Gillespie), and R15 DC014843 (J.G.T.), the
47 Howard Hughes Medical Institute (T.N.), the Amelia Peabody Charitable Fund (L.S.), NIH/NIDCD
48 intramural research funds 1ZIADC000085-01 (K.S.K.), and ZICDC000081 (R.S.P. and Y.W.), and a
49 Wellcome Trust grant 102892 (W.M.). We would like to acknowledge Catherine Weisz, Katie
50 Drerup, and Cole Graydon for their thoughtful comments on the manuscript.

51 **ABSTRACT**

52 In sensory hair cells of auditory and vestibular organs, the ribbon synapse is required for the
53 precise encoding of a wide range of complex stimuli. Hair cells have a unique presynaptic
54 structure—the synaptic ribbon—that organizes both synaptic vesicles and calcium channels at
55 the active zone. Previous work has shown that hair-cell ribbon size is correlated with
56 differences in postsynaptic activity. However, additional variability in postsynapse size presents
57 a challenge to determining the specific role of ribbon size in sensory encoding. To selectively
58 assess the impact of ribbon size on synapse function, we examined hair cells in transgenic
59 zebrafish that have enlarged ribbons, without postsynaptic alterations. Morphologically, we
60 found that enlarged ribbons had more associated vesicles and reduced presynaptic calcium-
61 channel clustering. Functionally, hair cells with enlarged ribbons had larger global and ribbon-
62 localized calcium currents. Afferent neuron recordings revealed that hair cells with enlarged
63 ribbons resulted in reduced spontaneous spike rates. Additionally, despite larger presynaptic
64 calcium signals, we observed fewer evoked spikes with longer latencies from stimulus onset.
65 Taken together, our work indicates that hair-cell ribbon size influences the spontaneous spiking
66 and the precise encoding of stimulus onset in afferent neurons.

67

68 **Significance statement**

69 Numerous studies support that hair-cell ribbon size corresponds with functional sensitivity
70 differences in afferent neurons and, in the case of inner hair cells of the cochlea, vulnerability
71 to damage from noise trauma. Yet it is unclear whether ribbon size directly influences sensory
72 encoding. Our study reveals that ribbon enlargement results in increased ribbon-localized
73 calcium signals, yet reduces afferent spontaneous activity and disrupts the timing of stimulus
74 onset—a distinct aspect of auditory and vestibular encoding. These observations suggest that
75 varying ribbon size alone can influence sensory encoding, and give further insight into how hair
76 cells transduce signals that cover a wide dynamic range of stimuli.

77

78

79 **INTRODUCTION**

80 Hair cells, the sensory receptors of auditory, vestibular, and lateral-line organs, utilize
81 specialized ribbon synapses to encode the timing and intensity of sensory information. Hair-cell
82 ribbon synapses are capable of rapid neurotransmitter release within milliseconds of stimulus
83 onset, and sustained neurotransmitter release over many seconds and longer (Parsons et al.,
84 1994; Moser and Beutner, 2000; Matthews and Fuchs, 2010). What features enable the hair-
85 cell ribbon synapse to perform such fine tasks is not well understood.

86 Hair-cell ribbon synapses are defined by a unique presynaptic structure known as the
87 synaptic ribbon, which is a dense specialization that tethers glutamate-filled vesicles adjacent
88 to clusters of the presynaptic calcium channel $\text{Ca}_v1.3$ (Usukura and Yamada, 1987; Brandt et al.,
89 2005; Obholzer et al., 2008; Seal et al., 2008; Schmitz, 2009; Frank et al., 2010). The major
90 component of ribbons is Ribeye, a unique protein that is vital for the physical integrity and
91 function of ribbon synapses (Schmitz et al., 2000; Zenisek et al., 2004; Frank et al., 2010; Sheets
92 et al., 2011; Lv et al., 2016). The size and shape of ribbons vary depending on species and hair-
93 cell type, but it is unclear how these differences impact synapse function (Moser et al., 2006).
94 Ribbons have been shown to tether and stabilize vesicles at the presynaptic active zone (Smith
95 and Sjostrand, 1961; Khimich et al., 2005; Buran et al., 2010). The number of tethered vesicles
96 increases with larger ribbons (reviewed in Nouvian et al., 2006), although the functional
97 implications of the additional vesicles is not clear. Previous studies have also shown that hair-
98 cell ribbons are able to recruit $\text{Ca}_v1.3$ channels, indicating an intimate relationship between
99 these structures (Frank et al., 2010; Sheets et al., 2011, 2012; Wong et al., 2014; Lv et al., 2016).

100 In the mammalian auditory system, substantial work has been done to determine how
101 ribbon size, $Ca_v1.3$ channels, and vesicle populations ultimately impact sensory encoding.
102 Studies have shown that, in auditory inner hair cells (IHCs) are innervated by multiple afferent-
103 nerve fibers (Pfeiffer and Kiang, 1965; Liberman, 1982; Taberner and Liberman, 2005; Johnson
104 et al., 2008). There is evidence that synapses with larger ribbons and smaller postsynapses have
105 a low rate of spontaneous release and correspond to high-threshold nerve fibers, while
106 synapses with smaller ribbons and larger postsynapses show a higher rate of spontaneous
107 release and correspond to low-threshold nerve fibers (Liberman et al., 2011). Whether
108 differences in afferent activity are due to morphological differences at the postsynapse or at
109 the ribbon is not well understood. In auditory IHCs, larger ribbons have also been shown to
110 localize more $Ca_v1.3$ channels and have larger synaptic calcium signals compared to smaller
111 ribbons (Meyer et al., 2009; Ohn et al., 2016). Despite larger calcium signals, larger ribbons
112 were not correlated with more afferent activity, which has been attributed to a depolarizing
113 shift in calcium channel activation present at larger ribbons compared to smaller ribbons. (Ohn
114 et al., 2016). Overall, additional differences in $Ca_v1.3$ channel numbers and variability in the size
115 of the postsynapse across ribbons in IHCs makes it is difficult to isolate the impact of ribbon size
116 on auditory encoding.

117 To address how ribbon size influences hair-cell ribbon-synapse function, we used a
118 transgenic zebrafish line that overexpresses Ribeye and enlarges ribbons (Sheets et al., 2011).
119 Although hair-cell ribbons are enlarged in this transgenic line, there was no significant effect on
120 postsynaptic size. Using a multipronged approach, we used this transgenic line as a model to
121 understand how hair-cell ribbon size alters ribbon-synapse morphology and function. We

122 found, at the ultrastructural level, that enlarged ribbons have more associated synaptic vesicles
123 yet a similar number of docked vesicles. Functionally, both global and ribbon-localized calcium
124 signals are increased in hair cells with enlarged ribbons. Despite increased calcium signaling,
125 presynaptic $Ca_v1.3$ channel density does not appear to scale up with ribbon enlargement, and
126 channel density is reduced. Despite increases in calcium current and more associated vesicles,
127 ribbon enlargement resulted in a reduction in spontaneous action potentials, and a longer
128 latency to fire following stimulus onset.

129

130 **MATERIALS AND METHODS**

131 *Fish Strains and Reagents.* Adult zebrafish (*Danio rerio*) were maintained with a 14-hour light,
132 10-hour dark cycle using standard methods. Zebrafish work performed at the NIH was approved
133 by the Animal Use Committee at the NIH under animal study protocol #1362-13. At Oregon
134 Health and Sciences University, zebrafish work was overseen by the Institutional Animal Care
135 and Use Committee. At Massachusetts Eye and Ear, zebrafish work was performed with the
136 approval of the Massachusetts Eye and Ear Animal Care Committee and in accordance with NIH
137 guidelines for use of zebrafish, protocol #13-001A. All zebrafish work at the University of
138 Sheffield was licensed by the UK Home Office under the Animals (Scientific Procedures) Act
139 1986 and approved by the University of Sheffield Ethical Review Committee. Larvae were
140 examined at 3-7 day post fertilization (dpf) unless stated otherwise. At these ages sex cannot be
141 predicted or determined, and therefore sex of the animal was not considered in our studies.
142 Zebrafish larvae were raised in E3 embryo media in mM: 5 NaCl, 0.17 KCl, 0.33 $CaCl_2$ and 0.33
143 $MgSO_4$, buffered in HEPES, at 30°C. All wild-type controls were non-transgenic siblings unless

144 stated otherwise. Previously described transgenic zebrafish strains used in this study include:

145 *Tg(-6myo6b:ribeye b-EGFP)^{vo67Tg}*, *Tg(-6myo6b:RGECO)^{vo10Tg}* and *Tg(-6myo6b:GCaMP6s-*

146 *CAAX)^{idc1Tg}* (Sheets et al., 2011; Maeda et al., 2014; Jiang et al., 2017).

147 *Vector Construction and Transgenic Lines.* To create additional Ribeye transgenic fish,
148 plasmid construction was based on the tol2/Gateway zebrafish kit developed by the lab of Chi-
149 Bin Chien at the University of Utah (Kwan et al., 2007). *Ribeye a* (NCBI Accession Number
150 [NM_001195491.1](#)) and *Ribeye b* ([NM_001015064.1](#)) were cloned into the middle entry vector
151 pDONR221 to create pME-*ribeye a* or pME-*ribeye b*. From the tol2 kit, vectors p3E-*mCherry*
152 (388), pDestTol2 (395, 394) and p3E-polyA (302) were recombined with p5E-*-6myosin6b* (Kindt
153 et al., 2012), and our engineered plasmids to create the following constructs: *-6myosin6b:ribeye*
154 *a-mCherry*, and *-6myosin6b:ribeye b-mCherry*.

155 To generate transgenic fish from these constructs, plasmid DNA (25-50 ng/μl) along with
156 *tol2* transposase mRNA (25-50 ng/μl) was injected into zebrafish embryos at the single-cell
157 stage. Transgenic lines were screened in the F1 and F2 generation for single copy integrations
158 and expression level. The *Tg(-6myo6b:ribeye b-mCherry)^{idc3Tg}* transgenic strain was selected
159 because using immunolabel (see methods below), it had normal number and size of ribbons
160 compared to wild-type (ribbon area normalized to the wild-type median area, wild-type: 0.924
161 ± 0.073 a.u., n = 245 ribbons; *ribeye b-mCherry*: 0.909 ± 0.051 a.u., n = 264 ribbons, p = 0.867;
162 synapses per hair cell via immunolabel: wild-type: 3.06 ± 0.13, n = 8 neuromasts; *ribeye b-*
163 *mCherry*: 2.97 ± 0.14, n = 6 neuromasts, p = 0.601). *Tg(-6myo6b:ribeye a-mCherry)^{idc2Tg}* was
164 chosen because similar to the *Tg(-6myo6b:ribeye b-EGFP)^{vo67Tg}* transgenic strain, two copies of
165 *Tg(-6myo6b:ribeye a-mCherry)^{idc2Tg}* resulted in ribbons that were significantly enlarged

166 compared to wild-type (ribbon area normalized to the wild-type median area, wild-type: 0.924
 167 ± 0.073 a.u., n = 245 ribbons; *ribeye a-mCherry X 2*: 1.90 ± 0.190 a.u., n = 377 ribbons, p =
 168 0.0006; synapses per hair cell via immunolabel: wild-type: 3.06 ± 0.13 n = 8 neuromasts; *ribeye*
 169 *a-mCherry X 2*: 2.86 ± 0.14 , n = 8 neuromasts, p = 0.304). This analysis was performed on z-stack
 170 images acquired on a Zeiss LSM780 microscope (see methods below). All Ribeye transgenic fish
 171 used in this study had a similar number of hair cells, and a normal startle reflex and balance,
 172 indicating that our transgenes do not overtly alter auditory or vestibular function.

173 For electron microscopy, immunohistochemistry, whole-cell recordings and afferent
 174 recordings, an incross of *Tg(-6myo6b:ribeye b-EGFP)^{vo67Tg}* was used to compare larvae with 2
 175 copies of Ribeye b-EGFP to wild-type, nontransgenic siblings. For cytosolic calcium
 176 measurements, *Tg(-6myo6b:RGECO1)^{vo10Tg}*; *Tg(-6myo6b:ribeye b-EGFP)^{vo67Tg} X 2* triple
 177 transgenic hair cells were compared to *Tg(-6myo6b:RGECO1)^{vo10Tg}* single transgenic hair cells.
 178 For ribbon-localized calcium responses, *Tg(-6myo6b:GCaMP6s-CAAX)^{idc1Tg}*; *Tg(-6myo6b:ribeye*
 179 *a-mCherry)^{idc2Tg} X 2* triple transgenic hair cells with enlarged ribbons were compared to *Tg(-*
 180 *6myo6b:GCaMP6s-CAAX)^{idc1Tg}*; *Tg(-6myo6b:ribeye b-mCherry)^{idc3Tg}* double transgenic hair cells
 181 with wild-type sized ribbons.

182 *Zebrafish Immobilization and Hair Cell Mechanical Stimulation.* To suppress muscle
 183 activity, larvae were anesthetized with 0.03% 3-amino benzoic acid ethyl ester (MS-222,
 184 Western Chemical, WA, USA), mounted with tungsten pins, and microinjected in the heart with
 185 125 μ M α -bungarotoxin (Tocris, Bristol, UK) to suppress muscle activity. Larvae were then
 186 rinsed and maintained in normal extracellular solution in mM: 130 NaCl, 2 KCl, 2 CaCl₂, 1 MgCl₂
 187 and 10 HEPES, pH 7.3, 290 mOsm. Stimulation of neuromast hair cells was performed as

188 described previously (Trapani and Nicolson, 2010). Briefly, we used a pressure clamp (HSPC-1,
189 ALA Scientific, New York) attached to a glass micropipette (inner tip diameter $\sim 30 \mu\text{m}$) filled
190 with normal extracellular solution to mechanically stimulate hair cells. The waterjet pipette was
191 positioned (MP-265, Sutter Instruments) approximately $100 \mu\text{m}$ from a given neuromast and
192 displacement ($3\text{-}5 \mu\text{m}$) of the kinocilia tips was verified by eye. For recordings of lateral-line
193 afferents, the pressure clamp was driven by a voltage command delivered by the recording
194 amplifier and pressure was monitored from a feedback sensor located on the HSPC-1 headstage
195 and collected concurrently. For calcium imaging experiments, the pressure clamp was driven by
196 a voltage step command. An outgoing voltage signal from the imaging software was used to
197 coordinate imaging with the pressure clamp stimulus.

198 *Electrophysiology, Lateral-line Afferent Recordings.* Our recording setup for action
199 currents has been described in detail (Trapani and Nicolson, 2010; Olt et al., 2016b). For all
200 experiments, recordings were performed in normal extracellular solution (see above) on
201 afferent neurons innervating zebrafish primary neuromasts (L1–L4). For extracellular
202 recordings, borosilicate glass pipettes were pulled (P-97, Sutter Instruments, Novato, CA) with a
203 long taper and had resistances between 5 and $15 \text{M}\Omega$ in extracellular solution. Signals were
204 collected with a Multiclamp 700B, a Digidata 1550 data acquisition board, along with pClamp10
205 software (Molecular Devices, LLC, Sunnyvale, CA). Extracellular currents were acquired from an
206 individual lateral-line afferent neuron in the loose-patch configuration (seal resistances ranged
207 from 20 to $80 \text{M}\Omega$ in extracellular solution). Recordings were done in voltage-clamp mode,
208 sampled at $50 \mu\text{s}/\text{pt}$, and filtered at 1 kHz. Spontaneous spike rate was quantified from
209 measurements of 500 spontaneous events per neuron. The innervated neuromast for a

210 recorded neuron was identified by progressively stimulating primary neuromasts of the
211 posterior lateral line until phase-locked spiking was detected.

212 *Electrophysiology, Lateral-line Hair-cell Recordings.* Whole-cell patch clamp experiments
213 were performed from hair cells of the zebrafish primary neuromasts (L1–L4) as previously
214 described (Olt et al., 2014, 2016b). The zebrafish were placed in a microscope chamber, with
215 continuous perfusion via a peristaltic pump in the following extracellular solution in mM: 135
216 NaCl, 1.3 CaCl₂, 5.8 KCl, 0.9 MgCl₂, 0.7 NaH₂PO₄, 5.6 D-glucose, 10 HEPES-NaOH. Sodium
217 pyruvate (2 mM), MEM amino acids solution (50X, without L-Glutamine) and MEM vitamins
218 solution (100X) were added from concentrates (Fisher Scientific, UK). The pH was 7.5. For
219 calcium current recordings, the extracellular solution was as the above but with 2.8 mM CaCl₂
220 instead of 1.3 mM (NaCl was reduced to 133 mM to keep the osmolality of the solution
221 constant).

222 Calcium current and changes in membrane capacitance recordings were conducted at
223 zebrafish body temperature (28.5°C). All other experiments (examination of K⁺ currents and
224 voltage responses) were performed at room temperature (21–24°C). Patch pipettes were made
225 from soda glass capillaries (Harvard Apparatus Ltd, Edenbridge, UK) and had a typical resistance
226 in the extracellular solution of 3–5 MΩ. To reduce the fast electrode capacitive transient, the
227 shank of each capillary was coated with surfboard wax (Mr. Zog's SexWax, Sexwax Inc.,
228 Carpinteria, CA, USA). Current and voltage recordings were performed using the following
229 intracellular solution in mM: 131 KCl, 3 MgCl₂, 1 EGTA-KOH, 5 Na₂ATP, 5 HEPES-KOH, and 10
230 sodium phosphocreatine, pH 7.3. For calcium current recordings and capacitance
231 measurements, the intracellular solution contained in mM: 85 Cs-glutamate, 20 CsCl, 3 MgCl₂, 1

232 EGTA-CsOH, 5 Na₂ATP, 5 Hepes-CsOH, 10 Na₂-phosphocreatine, 0.3 Na₂GTP, 15 4-
233 aminopyridine (4-AP), and 20 TEA, pH 7.3. Recordings were made with an Optopatch amplifier
234 (Cairn Research Ltd, Faversham, UK). Data acquisition was performed using pClamp software
235 with a Digidata 1322A data acquisition board (Molecular Devices, LLC, Sunnyvale, CA).
236 Recordings were sampled at 5 kHz or 100 kHz, low pass filtered at 2.5 kHz or 10 kHz (8-pole
237 Bessel) and stored on computer for offline analysis using Origin 2016 (OriginLab Corp.,
238 Northampton, MA, USA) and pClamp 10 (Molecular Devices, LLC, Sunnyvale, CA). Membrane
239 potentials in voltage clamp were corrected for the voltage drop across the uncompensated
240 residual series resistance (R_s : $5.3 \pm 0.5 \text{ M}\Omega$, $n = 56$) and for a liquid junction potential,
241 measured between electrode and bath solutions, of -4 mV for the KCl-based and -9 mV for Cs-
242 glutamate-based intracellular solution. Current responses are referred to a holding potential of
243 -84 mV or -79 mV , and are set to 0-current for easy comparison between recordings from
244 different hair cells.

245 *Calcium Imaging.* Optical measurements were made as previously described (Kindt et
246 al., 2012; Zhang et al., 2016). Briefly, calcium imaging experiments were performed in normal
247 extracellular solution (see above). Recordings were made at 10 Hz for cytosolic RGECO1
248 measurements and 20 Hz for ribbon-localized GCaMP6s-CAAX measurements. For cytosolic
249 calcium measurements using RGECO1, a Nikon Eclipse NiE widefield system with a 60 \times 1.0 NA
250 CFI Fluor water-immersion objective was used with excitation: 540/25 565LP and emission:
251 620/60 filters. The microscope was equipped with an Orca D2 camera (Hamamatsu,
252 Hamamatsu City, Japan), controlled using Elements software (Nikon Instruments Inc., Melville,
253 NY). For cytosolic RGECO1 measurements, a central imaging plane at the level of hair cell

254 nucleus was used. Calcium measurements at presynaptic ribbons made using GCaMP6s-CAAX
255 were acquired on a Swept-field confocal system built on a Nikon FN1 upright microscope
256 (Bruker Corporation, Billerica, MA) with a 60× 1.0 NA CFI Fluor water-immersion objective. The
257 microscope was equipped with a Rolera EM-C2 EMCCD camera (QImaging, Surrey, Canada),
258 controlled using Prairie view (Bruker Corporation, Billerica, MA). GCaMP6s-CAAX and Ribeye-
259 mCherry were excited using 488 and 561 nm solid state lasers. The microscope was equipped
260 with a Dual-View beam splitter (Photometrics, Tucson, AZ) using the following filters: dichroic
261 565; GCaMP6 emission 520/30; mCherry emission 630/50 (Chroma, Bellows Falls, VT) to enable
262 dual imaging of GCaMP6s-CAAX calcium signals and Ribeye-mCherry to detect ribbon location.
263 The Ribeye-mCherry signal was used to select a GCaMP6s-CAAX imaging plane containing
264 ribbons in multiple hair cells. For comparisons, calcium imaging experiments were done using a
265 minimum of 4 animals and 8 neuromasts per group.

266 The L-type calcium channel antagonist isradipine (Sigma-Aldrich, St. Louis, MO) was
267 prepared in normal extracellular solution with 0.1 % dimethyl sulfoxide (DMSO) and used at 10
268 μ M. Larvae were incubated in drugs for 10 min prior to calcium imaging.

269 *Transmission Electron Microscopy.* For electron microscopy, 4 dpf wild-type siblings and
270 *ribeye b-EGFP* transgenic larvae were fixed in freshly prepared 2% paraformaldehyde and 4%
271 glutaraldehyde (Electron Microscopy Sciences (EMS), Hatfield, PA) in 0.1 M phosphate buffer
272 pH 7.4 for 30 minutes at room temperature, followed by a 2 hour incubation at 4°C. Larvae
273 were washed with 0.1 M cacodylate buffer 3x5 min, and then fixed in 2% glutaraldehyde for 15
274 min, and washed again with 0.1 M cacodylate buffer 3x5 min. Larvae were then placed in 0.1 M
275 osmium tetroxide buffer for 30 min and then washed with 0.1 M cacodylate buffer 3x10 min.

276 Larvae were then dehydrated in ethanol: 3x5 min 50% ethanol, 15 min 50% ethanol with 1%
277 uranyl acetate, then 2x5 min 75% ethanol, 1x10 min 95% ethanol, 3x10 min 100% ethanol.
278 After dehydration, larvae were placed in propylene oxide (PO), and the incubated in Epon:PO ::
279 1:1 for 1 hour, Epon:PO :: 2:1 for 1 hour, and lastly pure Epon overnight. Epon embedded
280 samples were then placed in an oven at 64°C for 24 hours. Transverse serial sections (60–80 nm
281 thin sections were placed on a single-slot, formvar/carbon coated nickel grid, 2x1 mm-EMS,
282 Hatfield, PA) were used to section through cranial neuromasts located between the eyes, or
283 neuromasts located between the eye and the ear. Samples were imaged on a JEOL JEM-2100
284 electron microscope (JEOL Inc., Tokyo, Japan). Whenever possible, serial sections were used to
285 restrict our analysis to central sections of ribbons that were directly adjacent to a plasma
286 membrane and near a well-defined afferent postsynaptic density. For our analysis, we analyzed
287 6 *ribeye b-EGFP* and 9 wild-type neuromasts, examining up to 7 sections per neuromast.
288 Micrographs containing ribbons were scored blinded. Vesicles with a diameter of 30–50 nm and
289 adjacent (within 60 nm of the ribbon) to the filamentous “halo” surrounding the ribbon were
290 counted as tethered vesicles. Readily releasable vesicles were defined as vesicles between the
291 ribbon and the plasma membrane. The distance of tethered vesicles from the ribbon was
292 defined as the linear distance between the edge of a vesicle and the point on the ribbon closest
293 to it. Average distance was calculated from five independent measurements of tethered, but
294 not readily releasable, vesicles around the perimeter of a ribbon. All distances and perimeters
295 were measured in ImageJ (Schneider et al., 2012).

296 *Whole-Mount Immunohistochemistry.* Zebrafish larvae were fixed with 4%
297 paraformaldehyde and 4% sucrose in phosphate buffer with 0.2 mM CaCl₂ for 4.5-6 hrs at 4°C.

298 Larvae were then permeabilized with ice cold acetone for 5 min, and blocked with PBS buffer
299 containing 2% goat serum, 1% bovine serum albumin (BSA), and 1% DMSO. Primary antibodies
300 were diluted in PBS buffer containing 1% BSA and 1% DMSO, and larvae were incubated in the
301 solution overnight at 4°C. Custom made primary antibodies for Ribeye a (rabbit polyclonal,
302 1:500), Ribeye b (IgG2a, 1:2000), and Cav1.3a (rabbit polyclonal, 1:1000), and a commercially
303 available antibody for Membrane-associated Guanylate Kinases (MAGUK, IgG1, 1:500,
304 NeuroMab AB_10698179) have been described and used previously (Sheets et al., 2011). After
305 removal of primary antibodies, diluted secondary antibodies coupled to Alexa 488, Alexa 647
306 (Life Technologies, Carlsbad, CA), or DyLight 549 (Jackson ImmunoResearch, West Grove, PA)
307 were added. Hair-cell nuclei were labeled with DAPI (Life Technologies, Carlsbad, CA).

308 *Confocal Imaging.* Confocal images of fixed samples were obtained as previously
309 described (Sheets et al., 2011). Briefly, z-stack images of whole neuromasts (spaced by 0.3 μm
310 over 5-10 μm) were acquired with an Olympus FV1000, a Leica SP8, or a Zeiss LSM780 confocal
311 microscope using 60x 1.3 NA oil, 63x 1.3 NA glycerol, or 63x 1.4 NA oil immersion objectives
312 respectively. For quantitative measurements, confocal imaging parameters, including gain, laser
313 power, scan speed, dwell time, resolution and zoom were maintained between comparisons.
314 For super resolution imaging (Figure 3F-G), a Zeiss LSM780 microscope with Airyscan was used
315 with a 63x 1.4 NA oil objective, a digital zoom of 25x, acquired at 256 X 256 in 0.19 μm sections.
316 Images were processed in Zen (Carl Zeiss, Jena, Germany) with an Airyscan processing factor of
317 6.0. For live images of samples (Figure 1A, 5A-B, 6A-B), a Nikon C2 (10x 0.3 NA air or 60x 1.0 NA
318 water objective) confocal system was used to image and excite EGFP, GCaMP6s, RGEKO or
319 mCherry using the appropriate solid-state laser. For each experiment, the microscope

320 parameters were adjusted using the brightest control specimen.

321 *Confocal Image Processing.* Maximal projections of z-stack confocal images were
322 created and analyzed using MetaMorph (Molecular Devices, LLC, Sunnyvale, CA) or ImageJ
323 software. Images containing immunolabel were corrected for background; within maximum-
324 intensity projections a $7 \mu\text{m}^2$ region containing the highest level of background was selected,
325 and the average-fluorescence intensity of that region was subtracted from each pixel within the
326 image stacks.

327 To quantitatively measure fluorescent intensities and areas of immunolabeled puncta in
328 Metamorph, individual neuromasts were delineated using the region tool, and between
329 comparisons, the same inclusive threshold was applied to isolate the pixels occupied by
330 immunolabeled puncta within the neuromast. A punctum was defined as a region of
331 immunolabel where the pixel intensity was at least threefold (Ribeye) or fivefold ($\text{Ca}_v1.3\text{a}$ and
332 MAGUK) above the average intensity measured in the whole neuromast. Once the appropriate
333 threshold was applied, the Integrated Morphometry Analysis function was used to
334 automatically quantify the number of puncta, the area of each immunolabeled punctum, and
335 the integrated intensity of fluorescent pixels within each individual punctum.

336 $\text{Ca}_v1.3\text{a}$ immunolabeled puncta adjacent or juxtaposing MAGUK immunolabel, i.e.
337 $\text{Ca}_v1.3\text{a}$ puncta that, due to the resolution limits of light microscopy, appeared to partially
338 overlap with MAGUK immunolabel (Sheets et al., 2012), were defined as presynaptic. To
339 determine if ribbons were adjacent to PSDs (postsynaptic densities), custom software written in
340 C++ was used as previously described (Lieberman et al., 2011) to produce, for each ribbon or
341 PSD, a thumbnail image of an x-y max-projection of a voxel cube ($1 \mu\text{m}^2$) extracted from

342 confocal image stacks and centered on each ribbon synapse using independently derived x, y,
343 and z coordinates of all ribbons and PSDs. The numbers of intact ribbon synapses i.e. ribbons
344 adjacent to PSDs were determined by visual inspection of these thumbnail arrays (see Figure
345 2C,D). Subsequent image processing for display within figures was performed using Photoshop
346 and Illustrator software (Adobe, San Jose, CA).

347 *Signal Analysis and Statistics.* Afferent electrophysiology data were analyzed using
348 custom software written in Igor Pro (Wavemetrics, Lake Oswego, OR) and were plotted with
349 Igor Pro and Prism 7 (Graphpad, La Jolla, CA). For calcium imaging, image registration and peak
350 detection were performed using custom scripts written in Matlab (The Mathworks, Natick, MA)
351 as described previously (Hilliard et al., 2005; Zhang et al., 2016). For RGECO1 calcium
352 measurements, a circular region of interest (ROI) with a diameter of 3 μm (215 nm per pixel)
353 was placed on each hair cell within a neuromast. For ribbon-localized GCaMP6s-CAAX
354 measurements, a circular ROI with a 1 μm diameter (268 nm per pixel) was placed on the
355 center of an individual ribbon. Ribbon location was determined by either simultaneous or
356 subsequent image capture of Ribeye-mCherry labeled ribbons.

357 Values in the text and data on graphs are expressed as mean \pm SEM. Whenever possible
358 an effort was made to minimize Type II error with appropriate population numbers. In some of
359 our more challenging electrophysiology experiments with low N values, we were not able to
360 achieve a power of >0.8 to indicate no significant difference. In these cases, we state, “we were
361 unable to detect differences” between the two populations. Where appropriate, datasets were
362 confirmed for normality using a Kolmogorov-Smirnov normality test, and for equal variances
363 using a F test to compare variances. Statistical significance between two conditions was

364 determined by either paired or unpaired, two-tailed Student's *t* tests, or a Mann-Whitney U
365 test, as appropriate. When multiple t-tests were performed on the same data, a Holm-Siadhk
366 method was used to correct for multiple comparisons.

367

368 **Results**

369 To examine how ribbon enlargement altered ribbon-synapse morphology and synapse
370 activity in hair cells, we took advantage of a transgenic zebrafish line with enlarged ribbons. In a
371 previous study, we created a stable transgenic line *Tg[myosin6b:ribeye b-EGFP]* that
372 overexpresses exogenous Ribeye b fused to EGFP in zebrafish inner ear hair cells and in
373 neuromast hair cells in the lateral-line system. Upon incrossing this transgenic strain, we
374 observed high levels of Ribeye b expression in hair cells (Figure 1A; expressing 2 copies and
375 subsequently referred to as *ribeye b-EGFP*) and substantially enlarged ribbons (Sheets et al.,
376 2011).

377 **Ribeye b-EGFP expressing hair cells have larger ribbons and more tethered synaptic vesicles**

378 Prior to investigating synaptic activity, we characterized the synaptic architecture of hair
379 cells with enlarged synapses and compared these measurements to wild-type synapses. We
380 examined TEM sections that featured ribbon bodies adjacent to postsynaptic densities in
381 zebrafish neuromasts from wild-type (*n* = 18) and *ribeye b-EGFP* transgenic (*n* = 19) ribbons. We
382 used TEM to quantify ribbon-body areas and found that ribbon areas were significantly larger
383 (2X) in *ribeye b-EGFP* hair cells compared to wild-type hair cells (Figure 1B-D,H; ribbon area,
384 wild-type: $0.065 \pm 0.009 \mu\text{m}^2$; *ribeye b-EGFP*: $0.138 \pm 0.023 \mu\text{m}^2$, *p* = 0.008).

385 We predicted that enlargement of ribbons would increase the number and distribution
386 of synaptic vesicles associated with the ribbon. Synaptic vesicles were defined as circular
387 structures 30-50 nm in diameter that were directly apposed to the filamentous halo
388 surrounding the ribbon body (Schnee et al., 2005; Obholzer et al., 2008). We observed a similar
389 vesicle density along wild-type and *ribeye b-EGFP* ribbon perimeters (Figure 1B-D,I; vesicle
390 density per 500 nm, wild-type: 12.07 ± 0.80 vesicles; *ribeye b-EGFP*: 11.79 ± 0.76 vesicles, $p =$
391 0.80). The average size of individual vesicles was also similar at wild-type and *ribeye b-EGFP*
392 ribbons (vesicle area, wild-type: $2236 \text{ nm}^2 \pm 129.1$; *ribeye b-EGFP*: $2345 \pm 73.7 \text{ nm}^2$, $p = 0.46$). In
393 contrast, we found that synaptic vesicles were slightly closer to the ribbon in *ribeye b-EGFP* hair
394 cells compared to wild-type (Figure 1B-D,L; vesicle to ribbon distance, wild-type: 55.52 ± 3.65
395 nm; *ribeye b-EGFP*: 45.43 ± 2.99 nm, $p = 0.039$), which indicates that vesicle tethering might be
396 slightly altered in the *ribeye b-EGFP* transgenic line. Importantly, our cross section
397 measurements revealed a significantly greater number of synaptic vesicles (1.3X more)
398 associated with *ribeye b-EGFP* ribbons compared to wild-type ribbons (Figure 1J; associated or
399 tethered vesicles, wild-type: 17.67 ± 1.58 vesicles; *ribeye b-EGFP*: 22.53 ± 1.57 vesicles, $p =$
400 0.036). However, we did not observe a significantly greater number of vesicles docked at the
401 active zones of enlarged ribbons, which we defined as vesicles beneath the ribbon and adjacent
402 to the plasma membrane that were also opposed to the postsynaptic density (Figure 1B-D,K;
403 docked vesicles, wild-type: 2.83 ± 0.62 ; *ribeye b-EGFP*: 2.74 ± 0.34 , $p = 0.890$). These results
404 indicate that enlarged ribbons in *ribeye b-EGFP* transgenic hair cells have significantly more
405 tethered vesicles but a similar number of docked synaptic vesicles compared to wild-type
406 ribbons.

407 In addition to larger ribbons associated with postsynaptic densities (synaptic ribbons),
408 we also observed ectopic ribbons in *ribeye b-EGFP* transgenic hair cells that were not associated
409 with postsynaptic densities (Figure 1E-G). Ectopic ribbons were rarely seen in wild-type TEM
410 sections; we observed over 60 ectopic ribbons in *ribeye b-EGFP* transgenic sections, but only 1
411 ectopic ribbon in a similar number of wild-type sections (n = 33 wild-type and n = 25 *ribeye b-*
412 *EGFP* sections). Overall, we determined that most ectopic ribbons were located above the
413 nucleus and were associated with membranous organelles or endosomes (Figure 1E-G). Only a
414 small subset of the ectopic ribbons were found along the membrane of hair cells (Figure 1E),
415 and the majority were associated with filaments in the cytosol (Figure 1F), or near the apical
416 cuticular plate of hair cells (Figure 1G). Together, our TEM studies revealed that overexpression
417 of Ribeye results in larger synaptic ribbons that are associated with more vesicles, as well as
418 additional ectopic ribbons that populate the hair-cell body.

419 **Enlarged ribbons do not affect postsynapse morphology or synapse number**

420 To assess whether ribbon enlargement also affected hair-cell postsynaptic morphology,
421 we used immunohistochemistry to examine the afferent postsynaptic densities (PSDs) at ribbon
422 synapses in lateral-line hair cells. We visualized afferent PSDs using an antibody against the
423 PSD-95 family of membrane-associated guanylate kinases (MAGUKs) and ribbons using
424 antibodies specific to both paralogs of zebrafish Ribeye—Ribeye a and Ribeye b (Sheets et al.,
425 2011). Because we observed numerous ectopic aggregates of Ribeye in our transgenic line
426 (Figure 1A, E-G; Figure 2B,D), we quantified only Ribeye and MAGUK immunolabel at ‘complete’
427 ribbon synapses, i.e. presynaptic Ribeye-labeled puncta juxtaposing MAGUK-labeled patches
428 (Figure 2C,D).

429 Because ribbon synapse components are too small to resolve accurately using
430 conventional confocal microscopy, we approximated the sizes of pre-and postsynaptic
431 components by examining the relative areas of Ribeye and MAGUK puncta. Corresponding to
432 our TEM results, the relative areas of Ribeye puncta were significantly larger within *ribeye b-*
433 *EGFP* hair cells compared to wild-type hair cells (Figure 2A-E; ribbon area (normalized to wild-
434 type median), wild-type: 1.082 ± 0.057 a.u., $n = 192$ ribbons; *ribeye b-EGFP*: 4.565 ± 0.252 a.u.,
435 $n = 132$ ribbons, $p < 0.0001$). By contrast, relative areas of MAGUK puncta were comparable to
436 wild-type (Figure 2A-E; PSD area (normalized to wild-type median), wild-type: 1.147 ± 0.059
437 a.u., $n = 192$ PSDs; *ribeye b-EGFP*: 1.311 ± 0.064 a.u., $n = 210$ PSDs, $p = 0.052$). We also
438 examined whether the amount of PSD protein was altered at *ribeye b-EGFP* postsynapses by
439 examining the integrated intensity of MAGUK immunolabel fluorescence per puncta, and found
440 that compared to *ribeye b-EGFP* puncta, amount of MAGUK within the PSDs was comparable to
441 wild-type puncta (MAGUK integrated intensity, wild-type: 18200 ± 1250 a.u., $n = 192$ PSDs;
442 *ribeye b-EGFP*: 20000 ± 1250 a.u., $n = 210$ PSDs, $p = 0.1884$). In addition, there was no
443 significant difference in the number of intact ribbon synapses between *rib b-EGFP* and wild-
444 type hair cells (Figure 2F; synapses per hair cell, wild-type: 2.44 ± 0.10 , $n = 11$ neuromasts;
445 *ribeye b-EGFP*: 2.32 ± 0.13 , $n = 12$ neuromasts, $p = 0.468$), and the PSDs appeared to correctly
446 localize adjacent to the ribbons (Figure 2B,D). These results indicate that enlarging the ribbon
447 via overexpression of Ribeye b does not proportionally affect PSD size, nor does it change the
448 number of ribbon synapses.

449 **Ca_v1.3a channels are less tightly clustered at enlarged ribbon synapses**

450 Previously, we reported that the voltage-gated calcium channel $Ca_v1.3$ —the presynaptic
451 calcium channel in mammalian and zebrafish hair cells—is localized to synaptic ribbons
452 (juxtaposing a PSD) and to ectopic aggregates of Ribeye b-EGFP (Figure 3B,B'; (Sheets et al.,
453 2011)). First, we determined whether $Ca_v1.3a$ distribution was affected at enlarged synaptic
454 ribbons. We reasoned that more tightly clustered $Ca_v1.3a$ immunolabeled puncta would, on
455 average, display higher average fluorescent intensities, and therefore examined the average
456 immunolabel intensity of $Ca_v1.3a$ puncta adjacent to a postsynapse. We found, at synapses
457 with enlarged synaptic ribbons, the average intensity of $Ca_v1.3a$ immunolabel was reduced
458 compared to wild-type synapses (Figure 3A-C; $Ca_v1.3a$ average intensity, wild-type: 11900 ± 205
459 a.u., $n = 282$ synapses; *ribeye b-EGFP*: 8930 ± 334 a.u., $n = 125$ synapses, $p < 0.0001$).
460 Interestingly, the integrated immunolabel intensity per puncta, which represents the total
461 amount of $Ca_v1.3a$ per synapse, was comparable between *ribeye b-EGFP* and wild-type
462 synapses (Figure 3D; $Ca_v1.3a$ integrated intensity, wild-type: $6.50 \times 10^5 \pm 0.38$ a.u., $n = 282$
463 synapses; *ribeye b-EGFP*: $1.08 \times 10^6 \pm 0.14$ a.u., $n = 125$ synapses, $p = 0.156$).

464 As our confocal imaging indicated $Ca_v1.3a$ labeling was less clustered at *ribeye b-EGFP*
465 synapses, we subsequently examined $Ca_v1.3a$ channel labeling more closely at synapses using
466 super resolution microscopy. We observed that $Ca_v1.3a$ channels appeared less clustered at
467 enlarged ribbons compared to wild-type ribbons (Figure 3F,G). Profile plots of $Ca_v1.3a$
468 immunolabel showed multiple peaks at wild-type synapses (Figure 3F'), corresponding with
469 clustered $Ca_v1.3a$ labeling at the ribbon (Figure 3F). In *ribeye b-EGFP* transgenic synapse,
470 $Ca_v1.3a$ labeling appeared more diffuse and spread out over a larger area (Figure 3G,G').

471 Collectively, these data suggest that there are a similar number of $\text{Ca}_v1.3a$ channels at enlarged
472 synaptic ribbons compared to wild-type, but the channels cluster at a lower density.

473 Similar to what we previously observed, in *ribeye b-EGFP* hair cells, there were many
474 additional ectopic ribbons with no associated PSD; these ectopic ribbons were also able to
475 recruit $\text{Ca}_v1.3a$ channels ((Sheets et al., 2011), Figure 3B,B'; example, see arrowhead). When we
476 summed the intensities of both ectopically and synaptically-localized $\text{Ca}_v1.3a$ immunolabel, we
477 observed significantly more overall $\text{Ca}_v1.3a$ present in *ribeye b-EGFP* transgenic hair cells
478 compared to wild-type hair cells (Figure 3E; total $\text{Ca}_v1.3a$ intensity per neuromast, wild-type:
479 $3.29 \times 10^5 \pm 0.47$ a.u., $n = 13$ neuromasts; *ribeye b-EGFP*: $5.03 \times 10^5 \pm 0.42$ a.u., $n = 14$
480 neuromasts, $p = 0.010$). These findings confirm that ectopic ribbons can recruit $\text{Ca}_v1.3a$ without
481 a postsynapse and suggest that the amount of $\text{Ca}_v1.3a$ allocated to each synaptic ribbon is
482 fixed. Perhaps, if the amount of $\text{Ca}_v1.3a$ at synaptic ribbons is fixed, then increases in Ribeye
483 and ribbon size can influence $\text{Ca}_v1.3a$ channel distribution and consequently serve as a
484 mechanism to adjust the overall density of $\text{Ca}_v1.3a$ channels at the active zone.

485 **Whole-cell calcium currents, but not capacitance measurements, are increased in hair cells**
486 **with enlarged ribbons**

487 To investigate how enlarged ribbons altered hair-cell function, we performed whole-cell
488 recordings from lateral-line hair cells of wild-type and of *ribeye b-EGFP* transgenic larvae. The
489 resting membrane potential of Ribeye b-EGFP expressing hair cells was similar to that measured
490 in wild-type hair cells (V_m , wild-type: -69.5 ± 4.8 mV, 3-5 dpf, $n = 4$; *ribeye b-EGFP*: -72.8 ± 3.8
491 mV, 3-5 dpf, $n = 6$, $p = 0.602$). In addition, at rest, we were unable to detect any difference in
492 cell membrane capacitance between genotypes (wild-type: 2.8 ± 0.3 pF, $n = 25$; *ribeye b-EGFP*:

493 3.3 ± 0.6 pF, $n = 31$, $p = 0.491$), which suggests that the overall size of the hair cells is similar.
494 Furthermore, there were no differences in the complement of K^+ currents, which included $I_{K,Ca}$
495 and I_A as previously described, between wild-type and *ribeye b-EGFP* hair cells (data not shown,
496 (Olt et al., 2014, 2016b).

497 Our immunolabel results indicate that the distribution of $Ca_v1.3a$ channels at *ribeye b-EGFP*
498 synapses is disrupted compared to wild-type synapses (Figure 3). We therefore examined
499 whether the calcium currents (I_{Ca}) expressed in *ribeye b-EGFP* hair cells were altered relative to
500 wild-type hair cells (Figure 4A,B). I_{Ca} was recorded using 2.8 mM extracellular calcium at 28.5°C,
501 and in the presence of the K^+ currents blockers 4-AP and TEA in the Cs-based intracellular
502 solution (see Methods, Figure 4A; example I_{Ca}). *Ribeye b-EGFP* hair cells had larger calcium
503 currents compared to wild-type hair cells (Figure 4B; at -31 mV, the peak of I_{Ca} , wild-type: -7.0
504 ± 1.4 pA, $n = 13$; *ribeye b-EGFP*: -13.2 ± 1.8 pA, $n = 10$, $p = 0.012$).

505 In hair cells, voltage-gated calcium currents are tightly associated with vesicle fusion, i.e.
506 exocytosis. To investigate whether *ribeye b-EGFP* hair cells had altered exocytosis, we
507 measured changes in cell-membrane capacitance (ΔC_m) following a 1.0-s depolarizing voltage
508 step (Figure 4C; example ΔC_m , (Moser and Beutner, 2000; Johnson et al., 2009; Olt et al., 2014,
509 2016a)). Despite the larger I_{Ca} in *ribeye b-EGFP* hair cells, the ΔC_m was similar to that measured
510 in wild-type cells (Figure 4C,D; ΔC_m 1.0-s step, wild-type: 9.0 ± 3.0 fF, $n = 6$; *ribeye b-EGFP*: $6.8 \pm$
511 1.0 fF, $n = 7$, $p = 0.47$), and similar to that reported in wild-type hair cells using the same
512 recording conditions (Olt et al., 2014, 2016b). These data show that, despite more associated
513 vesicles at enlarged ribbons and larger calcium currents in *ribeye b-EGFP* hair cells, the overall
514 amount of exocytosis does not correspondingly increase in response to a 1.0-s stimulus.

515 **Calcium imaging confirms larger cytosolic calcium responses in hair cells with enlarged**
516 **ribbons**

517 To further test calcium dynamics in hair cells with enlarged ribbons, we examined
518 mechanically-evoked calcium responses in a transgenic line expressing RGECO1 in hair cells
519 (Zhao et al., 2011; Maeda et al., 2014). RGECO1 is a red-shifted calcium indicator that enabled
520 us to spectrally separate Ribeye b-EGFP and RGECO1 and examine calcium responses within the
521 cytosol of hair cells with enlarged ribbons (Figure 5B; RGECO1 plus 2 copies of *ribeye b-EGFP*)
522 and wild-type ribbons (Figure 5A; RGECO1 alone). After a 2.0-s step-wise deflection of the
523 cupula of neuromasts, we measured and quantified mechanically-evoked calcium responses
524 (fluorescence response, $\Delta F/F_0$), in both genotypes. On average, calcium responses were
525 significantly larger in hair cells with enlarged ribbons compared to wild-type hair cells (Figure
526 5C,D; RGECO1 $\Delta F/F_0$, wild-type: 14.39 ± 1.03 %, $n = 54$ hair cells; *ribeye b-EGFP*: 21.89 ± 2.32 %, $n = 55$ hair cells, $p = 0.02$). This finding is consistent with what we observed in our whole-cell
528 calcium current measurements, where hair cells with enlarged ribbons had significantly larger
529 calcium currents. In addition to increased mechanically-evoked calcium responses, we also
530 observed that baseline calcium levels, as measured by baseline RGECO1 intensity, were
531 significantly elevated in *ribeye b-EGFP* transgenic hair cells compared to wild-type hair cells
532 (Figure 5E; RGECO1 baseline, wild-type: 610.9 ± 18.01 a.u., $n = 74$ hair cells; *ribeye b-EGFP*;
533 916.0 ± 28.62 a.u., $n = 96$ hair cells, $p < 0.0001$). Overall, elevated baseline calcium and
534 increased cytosolic calcium responses support the results from our whole-cell recordings, and
535 indicate that hair cells with enlarged ribbons have increased calcium signaling.

536 **Local calcium signals at ribbons are larger in hair cells with enlarged ribbons**

537 Our immunohistochemistry data indicate there are the same number of $\text{Ca}_v1.3a$ channels
538 at enlarged ribbons compared to wild-type ribbons, but the channels cluster at a lower density.
539 Functionally, our whole-cell recordings and cytosolic calcium imaging results show larger global
540 calcium responses in *ribeye b-EGFP* hair cells. To determine whether reduced $\text{Ca}_v1.3a$ channel
541 clustering altered the local calcium responses at enlarged synaptic ribbons, we established a
542 method to detect ribbon-localized calcium responses at ribbons. To do this, we used a
543 transgenic zebrafish that expresses the calcium indicator GCaMP6s (Chen et al., 2013) in hair
544 cells, localized to the plasma membrane with a CAAX motif (Figure 6A-C, (Jiang et al., 2017)).
545 We predicted that this line could be used to detect presynaptic calcium signals adjacent to
546 ribbons. To test this prediction, we created an additional transgenic line, *ribeye b-mCherry* that
547 has wild-type sized ribbons (see Methods) to mark ribbon location in order to measure
548 GCaMP6s-CAAX, ribbon-localized calcium signals. Using this double transgenic line (Figure 6A),
549 we were able to measure robust, mechanically-evoked calcium responses (fluorescence
550 response, $\Delta F/F_0$) basally in hair cells, in response to deflection of the cupula of neuromasts
551 (Figure 6C,C'). The presynaptic calcium signals were localized within a focal hotspot located at
552 ribbons (Figure 6C,C'). We detected ribbon-localized calcium signals by centering a region of
553 interest (ROI) with a 1 μm diameter over an individual ribbon (Figure 6C). Compared to an
554 adjacent ROI, calcium signals at the ribbon were greater (peak GCaMP6s calcium response for a
555 2.0-s stimulus, on ribbon: 158.10 ± 0.23 %; off ribbon: 32.08 ± 0.04 %, $n = 12$ hair cells, $p <$
556 0.0001 , examples shown in Figure 6C,C'). All presynaptic signals were blocked below detection
557 by application of the L-type calcium channel antagonist isradipine, with complete block
558 observed in 12/12 cells in response to a saturating stimulus (see example dashed traces in

559 Figure 6C'). Together, our imaging and pharmacological results support the use of GCaMP6s-
560 CAAX for detecting local, $\text{Ca}_v1.3\text{a}$ -dependent calcium signals at ribbons.

561 Due to spectral overlap between EGFP and GCaMP6s, the *ribeye b-EGFP* and *GCaMP6s-*
562 *CAAX* transgenic lines are not compatible for imaging. To overcome this obstacle, we created an
563 additional transgenic line with high levels of Ribeye expression. Instead of EGFP, we fused
564 Ribeye to mCherry. Similar to the *ribeye b-EGFP* transgenic line, when incrossed, *ribeye a-*
565 *mCherry* transgenic ribbons were enlarged compared to wild-type ribbons (see Methods and
566 Figure 6B). This enlargement is not observed in our control *ribeye b-mCherry* transgenic line,
567 where ribbon size is comparable to wild-type (see Methods and Figure 6A). We used these two
568 mCherry lines to mark ribbon position and determine if ribbon-localized calcium signals (using
569 *GCaMP6s-CAAX*) were altered at enlarged ribbons (*ribeye a-mCherry X 2*) compared to control
570 ribbons (*ribeye b-mCherry*). We found, during a 0.5-s step stimulus, that the magnitude of the
571 ribbon-localized calcium responses at enlarged ribbons was similar compared to control (Figure
572 6D). We reasoned that the GCaMP6s-CAAX indicator could become saturated during this
573 stimulus. Therefore, we also measured the magnitude of the ribbon-localized calcium response
574 during a shorter, 0.1-s step stimulus. During a 0.1-s step, we observed that calcium responses
575 were larger at enlarged ribbons when compared to control ribbons (Figure 6E,E'; peak
576 GCaMP6s ribbon calcium response, *ribeye b-mCherry* (WT): 36.94 ± 7.69 %, $n = 27$ ribbons;
577 *ribeye a-mCherry* (enlarged): 65.89 ± 11.27 %, $n = 29$ ribbons, $p = 0.042$). In addition, for the
578 0.1-s step stimulus, the slope (rate of change toward peak) of the response was increased at
579 enlarged ribbons compared to control (Figure 6E''; slope, *ribeye b-mCherry* (WT): 228.8 ± 45.04 ,
580 $n = 27$ ribbons; *ribeye a-mCherry* (enlarged): 407.2 ± 65.41 , $n = 29$ ribbons, $p = 0.041$).

581 In addition to synaptic ribbons, we also examined GCaMP6s-CAAX responses at ectopic
582 ribbons. We observed that despite associating with $Ca_v1.3a$ channels (Figure 3B,B'), at ectopic
583 ribbons, we were not able to measure a GCaMP6s-CAAX signal that was substantially different
584 from the surrounding background ($n = 15$ ectopic ribbons). This suggests that ectopic ribbons
585 may not contribute to the differences in global calcium signals that we measured using whole-
586 cell recordings or the calcium indicator RGECO1.

587 Overall, our measurements indicate that for short stimuli, ribbon-localized calcium
588 responses at enlarged synaptic ribbons are both faster and larger when compared to responses
589 at wild-type-sized synaptic ribbons. An increase in calcium signals at enlarged ribbons is in line
590 with our measurements of whole-cell calcium currents and our experiments using cytosolic
591 RGECO1 where we observed increased calcium responses. Taken together, these results
592 indicate that both local ribbon-localized calcium dynamics as well as global calcium dynamics
593 are increased with ribbon enlargement.

594 **Ribbon enlargement alters spontaneous and evoked afferent activity**

595 Presynaptic measurements of capacitance changes to estimate exocytosis were unable to
596 detect any differences in evoked neurotransmission between hair cells from wild-type or *ribeye*
597 *b-EGFP* transgenic fish. Due to the limited number of ribbons and associated vesicles in
598 zebrafish hair cells, it is likely that a large depolarizing stimulus may be required to detect
599 changes in exocytosis using capacitance measurements. This could confound our ability to
600 detect subtle differences in vesicle fusion between genotypes. Therefore, we examined
601 whether postsynaptic activity was affected in *ribeye b-EGFP* transgenic fish by performing
602 extracellular recordings of action currents from the cell bodies of the afferent neurons that

603 innervate lateral-line hair cells (Trapani and Nicolson, 2010). For these recordings, both
604 spontaneous and evoked action currents (spikes) are generated by neurotransmitter release
605 from hair cells that is dependent on $\text{Ca}_v1.3a$ activity (Trapani and Nicolson, 2011; Olt et al.,
606 2016b). Spontaneous spikes result from a receptor potential that is within the activation range
607 of $\text{Ca}_v1.3a$ channels when the hair cell is not stimulated. Evoked spikes occur when hair cells are
608 stimulated and result from depolarizing mechanotransduction currents that lead to rapid
609 activation of $\text{Ca}_v1.3a$ channels (Moser and Beutner, 2000; Jørgensen and Kroese, 2005; Trapani
610 and Nicolson, 2011).

611 Using our whole-animal, *in vivo* approach, we examined spontaneous and evoked activity
612 from afferent neurons of wild-type and *ribeye b-EGFP* transgenic fish. We first examined the
613 spontaneous activity of single afferent neurons and found that hair cells with enlarged ribbons
614 displayed significantly reduced rates of spontaneous activity with corresponding larger
615 interspike intervals (ISI) compared to wild-type hair cells (Figure 7A,B; spontaneous ISI, wild-
616 type: 0.147 ± 0.031 s, $n = 19$ cells; *ribeye b-EGFP*: 0.416 ± 0.085 s, $n = 18$ cells, $p = 0.0006$). This
617 result suggests that, despite having more synaptic vesicles localized to larger ribbons compared
618 to wild-type ribbons, *ribeye b-EGFP* transgenic hair cells have a lower probability of vesicle
619 fusion at rest.

620 We next examined evoked afferent activity to determine whether ribbon size played a
621 role in the encoding of mechanical stimuli. Stimuli were presented as two different types of
622 neuromast cupula deflections: a 200-ms sine wave at 20 Hz and a 500-ms square-step stimulus.
623 During a 20 Hz sine wave stimulus, we observed fewer spikes during two phases of the stimulus
624 that activated hair cells in *ribeye b-EGFP* larvae compared to wild-type larvae (Figure 7C,D). In

625 contrast, during a 500-ms step stimulus, we were unable to detect a difference in the average
626 number of spikes in *ribeye b-EGFP* afferents compared to wild-type afferents (Figure 7F,G;
627 spikes per 500-ms step, wild-type: 8.84 ± 1.86 spikes, $n = 11$ cells; *ribeye b-EGFP*: 7.64 ± 1.19
628 spikes, $n = 11$ cells, $p = 0.67$). These results are consistent with our capacitance measurements
629 where we observed no difference between *ribeye b-EGFP* transgenic and wild-type hair cells
630 after 1.0-s step stimuli (Figure 4C,D). When reconciling why the number of spikes were reduced
631 for 20 Hz, but not the 500-ms step stimulus, we noted that there were fewer spikes during the
632 first 25 ms of the 500-ms step in *ribeye b-EGFP* transgenic fish compared to wild-type (Figure
633 7H; wild-type: 2.26 ± 0.26 spikes, $n = 11$ cells; *ribeye b-EGFP*: 1.35 ± 0.60 spikes, $n = 11$ cells, $p =$
634 0.022). This initial reduction of spikes suggests that fewer vesicles fuse at enlarged ribbons
635 during the onset of a stimulus. For the 20 Hz sine-wave stimulus, the depolarizing phase of each
636 50-ms cycle (labeled A-D for the 200-ms stimulus duration in Figure 7C) is 25 ms, which may not
637 be enough time for enlarged ribbons to achieve wild-type levels of exocytosis. Together, the
638 decrease in afferent activity in response to short-phasic 20 Hz stimuli and at the onset of a
639 longer-lasting saturating stimulus supports the hypothesis that there is reduced exocytosis at
640 enlarged ribbons at stimulus onset.

641 Our examination of encoding of stimulus onset also revealed that the mean of the first
642 spike latency (FSL) in response to a 500-ms step was longer in *ribeye b-EGFP* afferent neurons
643 compared to wild-type neurons (Figure 7I; first spike latency for a 500-ms step, wild-type: 9.47
644 ± 1.59 ms, $n = 11$ cells; *ribeye b-EGFP*: 23.40 ± 6.27 ms, $n = 11$ cells, $p = 0.007$). In addition, FSLs
645 appeared slightly longer for each phase of the 20 Hz sine-wave stimulus; however, these
646 individual values were not statistically different from wild-type (Figure 7E). Overall, hair cells

647 with enlarged ribbons resulted in a significantly reduced rate of spontaneous activity in
648 downstream afferent neurons, and an alteration in evoked activity with fewer postsynaptic
649 spikes and longer first spike latencies at stimulus onset.

650

651 **DISCUSSION**

652 A specific role for the synaptic ribbon in sensory encoding has been remarkably
653 challenging to define. Genetic studies aimed to perturb ribbons have yet to give a complete
654 story of what features enable ribbon synapses to encode a particular auditory or vestibular
655 stimulus. We used a transgenic zebrafish line that overexpresses Ribeye and enlarges hair-cell
656 ribbons in order to examine how ribbon size alters the morphology and function of hair-cell
657 synapses. Morphologically, hair cells with enlarged ribbons had more associated vesicles and
658 failed to tightly cluster presynaptic $\text{Ca}_v1.3a$ channels, while PSDs appeared unaltered.
659 Functionally, whole-cell calcium currents, cytosolic calcium responses, and ribbon-localized
660 calcium responses were larger in hair cells with enlarged ribbons. Despite increased calcium
661 signaling, enlarging ribbons resulted in reduced afferent spontaneous activity and disruptions in
662 evoked release at the onset of stimuli. Overall, our results suggest that alterations to
663 presynaptic ribbon size can influence postsynaptic activity and the encoding properties of
664 ribbon synapses.

665 **Ribeye and $\text{Ca}_v1.3$ channel clustering**

666 Numerous reports have shown that $\text{Ca}_v1.3$ channels are clustered beneath hair-cell
667 ribbons and are required for fast exocytosis at ribbon synapses (Frank et al., 2010; Moser and
668 Beutner, 2000; Roberts, 1994; Sheets et al., 2012; Wong et al., 2014). Two recent studies

669 examining the genetic reduction of Ribeye in zebrafish hair cells and mouse retina have also
670 indicated a close relationship between Ribeye levels and Ca_v1 localization. In these studies,
671 disruption of Ribeye levels resulted in mislocalization of $Ca_v1.3a$ and $Ca_v1.4$ respectively (Lv et
672 al., 2016; Maxeiner et al., 2016). We also observed a strong association between $Ca_v1.3a$ and
673 Ribeye; $Ca_v1.3a$ was recruited to all ribbons, including ectopic ribbons generated by
674 overexpression of Ribeye (Figure 3B,B'). Yet our observations in this study reveal that
675 augmenting Ribeye at synapses is not sufficient to recruit additional $Ca_v1.3a$ channels to
676 synapses. We observed that the number of $Ca_v1.3a$ at individual synaptic ribbons did not scale
677 up with increased Ribeye levels and ribbon enlargement. Instead, the integrated intensity of
678 $Ca_v1.3a$ channel immunolabel at enlarged synaptic ribbons was similar to wild-type (Figure 3D),
679 but spread out over larger ribbon areas (Figure 3A-D,F-G). This result suggests that Ca_v1 -
680 channel density at the synapse may be regulated independently of Ribeye, perhaps through
681 another ribbon-associated scaffolding protein such as Bassoon, or a RIM protein (Frank et al.,
682 2010; Jung et al., 2015).

683 **The ribbon's influence on coupling calcium influx and vesicle fusion**

684 Previous work compiled from TEM studies has shown that larger ribbons have more
685 ribbon-associated vesicles (Nouvian et al., 2006; Matthews and Fuchs, 2010; Graydon et al.,
686 2011). Likewise, our TEM data also indicate that enlarged ribbons have an increased number of
687 tethered vesicles compared to wild-type ribbons, which predicts the potential for an increase in
688 vesicle fusion (Figure 1J). In addition, our measurements of whole-cell calcium currents and
689 ribbon-localized calcium signals found that calcium responses were elevated in hair cells with
690 enlarged ribbons (Figure 4A,B, Figure 6E,E'). Yet despite larger calcium currents and more

691 tethered vesicles at enlarged ribbons, we observed no increase in evoked activity and a
692 significant reduction in spontaneous vesicle fusion (Figure 7). These results are similar to what
693 has been observed in mammalian auditory IHCs, where larger ribbons are correlated with
694 elevated calcium currents and less spontaneous activity (Taberner and Liberman, 2005;
695 Liberman et al., 2011)

696 Our results suggest that other presynaptic factors may be important to couple calcium
697 influx and vesicle fusion. There are several scenarios wherein ribbon enlargement could impact
698 this coupling and ultimately the probability of vesicle fusion driving both spontaneous and
699 evoked activity. These mechanisms include changes in $Ca_v1.3$ channel activation properties, an
700 inhibitory effect on vesicle release by the ribbon itself, and/or a disruption of coupling between
701 presynaptic calcium signaling and vesicle fusion.

702 Alterations to $Ca_v1.3$ channel activation threshold could result in decreased
703 spontaneous release and set a higher threshold for fusion of the vesicles at stimulus onset
704 (Brandt et al., 2005; Magistretti et al., 2015). Recent work in mouse IHCs found that, compared
705 to smaller ribbons, $Ca_v1.3$ channels at larger ribbons within the same hair cell were activated at
706 more depolarized membrane potentials creating a higher threshold for activation (Ohn et al.,
707 2016). By contrast, we saw a similar activation of the calcium current in transgenic hair cells
708 compared to wild-type hair cells (Figure 4B). Additionally, we did not observe differences in the
709 resting potential in our whole-cell recordings (see Results). Overall, our data support that the
710 reduced afferent activity we observed in our transgenic is not likely due to altered $Ca_v1.3a$
711 channel activation.

712 Another possibility is the physical size or composition of the ribbon could impact vesicle
713 fusion. For example, previous studies in bipolar cells suggest one function of the ribbon may be
714 to stabilize a group of vesicles for evoked release while minimizing their spontaneous release
715 (Zenisek, 2008; Vaithianathan et al., 2013). We did observe that overexpression of Ribeye
716 decreased the distance between tethered vesicles and the ribbon (Figure 1L), which provides
717 some evidence that Ribeye may play a role in vesicle tethering, and perhaps could act to
718 stabilize vesicles at the ribbon. If enlarged ribbons restrain vesicles and inhibit their release, this
719 mechanism could explain why we observed larger calcium currents (Figure 4A,B) and more
720 tethered vesicles (Figure 1J) in hair cells with enlarged ribbons, but less spontaneous afferent
721 activity and disruptions in evoked activity (Figure 7).

722 In addition to the physical size of the ribbon and the amount of Ribeye influencing
723 vesicle fusion, reduced $Ca_v1.3a$ channel clustering observed at enlarged ribbons (Figure 3F-G)
724 could impact the coupling of presynaptic calcium influx to vesicle fusion. Coupling of
725 presynaptic calcium influx to vesicle release in hair cells has been previously described by two
726 models. The first is the nanodomain model, in which the opening of one or a few $Ca_v1.3$
727 channels is coupled to exocytotic calcium sensors on adjacent vesicles that trigger fusion
728 (Brandt et al., 2005; Goutman and Glowatzki, 2007; Wong et al., 2014). In the second, the
729 microdomain model, the opening of several, more distant $Ca_v1.3$ channels is necessary to
730 collectively raise calcium levels to overcome mobile calcium buffering and drive vesicle fusion
731 (Roberts, 1994; Beaumont et al., 2005). Our current study was not designed to study the spread
732 of calcium at the presynapse; therefore our results cannot be used to conclusively distinguish
733 between either of these models. Regardless of the mechanism, it is possible that reduced

734 $Ca_v1.3$ channel clustering impacts the coupling of presynaptic calcium influx with vesicle fusion.
735 In future studies, it will be useful to design experiments using this transgenic line to directly
736 explore how enlarged ribbons affect the coupling of presynaptic calcium influx and vesicle
737 fusion in more detail.

738 **The relationship between ribbon size and afferent neuron sensitivity**

739 Ribbon size correlates with the sensitivity of auditory nerve fibers innervating IHCs of
740 the cochlea, with smaller ribbons associated with low-threshold/high-spontaneous rate fibers
741 and larger ribbons associated with high-threshold/low-spontaneous rate fibers (Taberner and
742 Liberman, 2005; Liberman et al., 2011). A recent study characterizing the firing properties of rat
743 auditory neurons supports that differences observed in afferent spike timing can be attributed
744 to the properties of presynaptic vesicle release mechanisms (Wu et al., 2016). When we
745 enlarged synaptic ribbons in the zebrafish lateral line, we observed a shift in afferent fiber
746 sensitivity; that is, enlarged ribbons resulted in a reduced rate of spontaneous firing in afferent
747 neurons (Figure 7A,B). This finding is consistent with the correlation described in IHCs,
748 suggesting that varying ribbon size may be a sufficient mechanism for tuning afferent
749 sensitivity.

750 In addition to reduced spontaneous spike rates in afferent neurons, enlarged ribbons
751 also resulted in an increase in first spike latency at stimulus onset. Moreover, we observed
752 decreases in evoked spikes in response to shorter-duration stimuli (20 Hz, 25-ms stimulus per
753 phase), and during the onset (first 25 ms) of longer, sustained stimuli. In larval zebrafish, the
754 fidelity and latency of the first spike is an important fast encoding mechanism utilized to rapidly
755 generate an escape reflex that can be critical for survival (Troconis et al., 2017). In mammals,

756 the first spike is important for perceptual encoding (Heil, 2004; Johansson and Birznieks, 2004;
757 Chase and Young, 2007) as well as sound localization (Furukawa and Middlebrooks, 2001).

758 Our observations in the zebrafish lateral line reveal that enlargement of ribbons in hair
759 cells is sufficient to alter afferent activity. This work provides insight into the mechanisms of
760 hair-cell synapse heterogeneity and suggests that hair cells could use a simple strategy—varying
761 ribbon size—to achieve sensitivity over a broad dynamic range of stimuli. It is possible that our
762 study is relevant from a clinical perspective, as recent work has found that ribbon enlargement
763 following moderate noise exposure is accompanied by coding deficits in auditory nerve fibers
764 (Song et al., 2016). It will be useful in future studies to determine if morphological changes to
765 hair-cell ribbons directly contribute to functional deficits associated with noise exposure.

766

767 **References**

- 768 Beaumont V, Llobet A, Lagnado L (2005) Expansion of calcium microdomains regulates fast
769 exocytosis at a ribbon synapse. *Proc Natl Acad Sci U S A* 102:10700–10705.
- 770 Brandt A, Khimich D, Moser T (2005) Few CaV1.3 channels regulate the exocytosis of a synaptic
771 vesicle at the hair cell ribbon synapse. *J Neurosci Off J Soc Neurosci* 25:11577–11585.
- 772 Buran BN, Strenzke N, Neef A, Gundelfinger ED, Moser T, Liberman MC (2010) Onset coding is
773 degraded in auditory nerve fibers from mutant mice lacking synaptic ribbons. *J Neurosci*
774 *Off J Soc Neurosci* 30:7587–7597.
- 775 Chase SM, Young ED (2007) First-spike latency information in single neurons increases when
776 referenced to population onset. *Proc Natl Acad Sci U S A* 104:5175–5180.
- 777 Chen T-W, Wardill TJ, Sun Y, Pulver SR, Renninger SL, Baohan A, Schreiter ER, Kerr RA, Orger
778 MB, Jayaraman V, Looger LL, Svoboda K, Kim DS (2013) Ultrasensitive fluorescent
779 proteins for imaging neuronal activity. *Nature* 499:295–300.
- 780 Frank T, Rutherford MA, Strenzke N, Neef A, Pangršič T, Khimich D, Fejtova A, Fejtova A,
781 Gundelfinger ED, Liberman MC, Harke B, Bryan KE, Lee A, Egnér A, Riedel D, Moser T
782 (2010) Bassoon and the synaptic ribbon organize Ca²⁺ channels and vesicles to add
783 release sites and promote refilling. *Neuron* 68:724–738.

- 784 Furukawa S, Middlebrooks JC (2001) Sensitivity of auditory cortical neurons to locations of
785 signals and competing noise sources. *J Neurophysiol* 86:226–240.
- 786 Goutman JD, Glowatzki E (2007) Time course and calcium dependence of transmitter release at
787 a single ribbon synapse. *Proc Natl Acad Sci U S A* 104:16341–16346.
- 788 Graydon CW, Cho S, Li G-L, Kachar B, Gersdorff H von (2011) Sharp Ca²⁺ Nanodomains beneath
789 the Ribbon Promote Highly Synchronous Multivesicular Release at Hair Cell Synapses. *J*
790 *Neurosci* 31:16637–16650.
- 791 Heil P (2004) First-spike latency of auditory neurons revisited. *Curr Opin Neurobiol* 14:461–467.
- 792 Hilliard MA, Apicella AJ, Kerr R, Suzuki H, Bazzicalupo P, Schafer WR (2005) In vivo imaging of *C.*
793 *elegans* ASH neurons: cellular response and adaptation to chemical repellents. *EMBO J*
794 24:63–72.
- 795 Jiang T, Kindt K, Wu DK (2017) Transcription factor Emx2 controls stereociliary bundle
796 orientation of sensory hair cells. *eLife* 6:e23661.
- 797 Johansson RS, Birznieks I (2004) First spikes in ensembles of human tactile afferents code
798 complex spatial fingertip events. *Nat Neurosci* 7:170–177.
- 799 Johnson SL, Forge A, Knipper M, Münkner S, Marcotti W (2008) Tonotopic Variation in the
800 Calcium Dependence of Neurotransmitter Release and Vesicle Pool Replenishment at
801 Mammalian Auditory Ribbon Synapses. *J Neurosci Off J Soc Neurosci* 28:7670–7678.
- 802 Johnson SL, Franz C, Knipper M, Marcotti W (2009) Functional maturation of the exocytotic
803 machinery at gerbil hair cell ribbon synapses. *J Physiol* 587:1715–1726.
- 804 Jørgensen F, Kroese ABA (2005) Ion channel regulation of the dynamical instability of the
805 resting membrane potential in saccular hair cells of the green frog (*Rana esculenta*).
806 *Acta Physiol Scand* 185:271–290.
- 807 Jung S, Oshima-Takago T, Chakrabarti R, Wong AB, Jing Z, Yamanbaeva G, Picher MM, Wojcik
808 SM, Göttfert F, Predoehl F, Michel K, Hell SW, Schoch S, Strenzke N, Wichmann C, Moser
809 T (2015) Rab3-interacting molecules 2 α and 2 β promote the abundance of voltage-gated
810 CaV1.3 Ca²⁺ channels at hair cell active zones. *Proc Natl Acad Sci* 112:E3141–E3149.
- 811 Khimich D, Nouvian R, Pujol R, Tom Dieck S, Egner A, Gundelfinger ED, Moser T (2005) Hair cell
812 synaptic ribbons are essential for synchronous auditory signalling. *Nature* 434:889–894.
- 813 Kindt KS, Finch G, Nicolson T (2012) Kinocilia mediate mechanosensitivity in developing
814 zebrafish hair cells. *Dev Cell* 23:329–341.
- 815 Kwan KM, Fujimoto E, Grabher C, Mangum BD, Hardy ME, Campbell DS, Parant JM, Yost HJ,
816 Kanki JP, Chien C-B (2007) The Tol2kit: a multisite gateway-based construction kit for

- 817 Tol2 transposon transgenesis constructs. *Dev Dyn Off Publ Am Assoc Anat* 236:3088–
818 3099.
- 819 Liberman LD, Wang H, Liberman MC (2011) Opposing Gradients of Ribbon Size and AMPA
820 Receptor Expression Underlie Sensitivity Differences among Cochlear-Nerve/Hair-Cell
821 Synapses. *J Neurosci* 31:801–808.
- 822 Liberman MC (1982) Single-neuron labeling in the cat auditory nerve. *Science* 216:1239–1241.
- 823 Lv C, Stewart WJ, Akanyeti O, Frederick C, Zhu J, Santos-Sacchi J, Sheets L, Liao JC, Zenisek D
824 (2016) Synaptic Ribbons Require Ribeye for Electron Density, Proper Synaptic
825 Localization, and Recruitment of Calcium Channels. *Cell Rep* 15:2784–2795.
- 826 Maeda R, Kindt KS, Mo W, Morgan CP, Erickson T, Zhao H, Clemens-Grisham R, Barr-Gillespie
827 PG, Nicolson T (2014) Tip-link protein protocadherin 15 interacts with transmembrane
828 channel-like proteins TMC1 and TMC2. *Proc Natl Acad Sci U S A* 111:12907–12912.
- 829 Magistretti J, Spaiardi P, Johnson SL, Masetto S (2015) Elementary properties of Ca²⁺ channels
830 and their influence on multivesicular release and phase-locking at auditory hair cell
831 ribbon synapses. *Front Cell Neurosci* 9:123.
- 832 Matthews G, Fuchs P (2010) The diverse roles of ribbon synapses in sensory neurotransmission.
833 *Nat Rev Neurosci* 11:812–822.
- 834 Maxeiner S, Luo F, Tan A, Schmitz F, Südhof TC (2016) How to make a synaptic ribbon: RIBEYE
835 deletion abolishes ribbons in retinal synapses and disrupts neurotransmitter release.
836 *EMBO J* 35:1098–1114.
- 837 Meyer AC, Frank T, Khimich D, Hoch G, Riedel D, Chapochnikov NM, Yarin YM, Harke B, Hell SW,
838 Egner A, Moser T (2009) Tuning of synapse number, structure and function in the
839 cochlea. *Nat Neurosci* 12:444–453.
- 840 Moser T, Beutner D (2000) Kinetics of exocytosis and endocytosis at the cochlear inner hair cell
841 afferent synapse of the mouse. *Proc Natl Acad Sci U S A* 97:883–888.
- 842 Moser T, Brandt A, Lysakowski A (2006) Hair cell ribbon synapses. *Cell Tissue Res* 326:347–359.
- 843 Nouvian R, Beutner D, Parsons TD, Moser T (2006) Structure and Function of the Hair Cell
844 Ribbon Synapse. *J Membr Biol* 209:153–165.
- 845 Obholzer N, Wolfson S, Trapani JG, Mo W, Nechiporuk A, Busch-Nentwich E, Seiler C, Sidi S,
846 Söllner C, Duncan RN, Boehland A, Nicolson T (2008) Vesicular glutamate transporter 3
847 is required for synaptic transmission in zebrafish hair cells. *J Neurosci Off J Soc Neurosci*
848 28:2110–2118.

- 849 Ohn T-L, Rutherford MA, Jing Z, Jung S, Duque-Afonso CJ, Hoch G, Picher MM, Scharinger A,
850 Strenzke N, Moser T (2016) Hair cells use active zones with different voltage
851 dependence of Ca²⁺ influx to decompose sounds into complementary neural codes.
852 Proc Natl Acad Sci U S A.
- 853 Olt J, Allen CE, Marcotti W (2016a) In vivo physiological recording from the lateral line of
854 juvenile zebrafish. J Physiol:n/a-n/a.
- 855 Olt J, Johnson SL, Marcotti W (2014) In vivo and in vitro biophysical properties of hair cells from
856 the lateral line and inner ear of developing and adult zebrafish. J Physiol 592:2041–
857 2058.
- 858 Olt J, Ordoobadi AJ, Marcotti W, Trapani JG (2016b) Physiological recordings from the zebrafish
859 lateral line. Methods Cell Biol 133:253–279.
- 860 Parsons TD, Lenzi D, Almers W, Roberts WM (1994) Calcium-triggered exocytosis and
861 endocytosis in an isolated presynaptic cell: Capacitance measurements in saccular hair
862 cells. Neuron 13:875–883.
- 863 Pfeiffer RR, Kiang NY (1965) Spike Discharge Patterns of Spontaneous and Continuously
864 Stimulated Activity in the Cochlear Nucleus of Anesthetized Cats. Biophys J 5:301–316.
- 865 Roberts WM (1994) Localization of calcium signals by a mobile calcium buffer in frog saccular
866 hair cells. J Neurosci Off J Soc Neurosci 14:3246–3262.
- 867 Schmitz F (2009) The making of synaptic ribbons: how they are built and what they do. Neurosci
868 Rev J Bringing Neurobiol Neurol Psychiatry 15:611–624.
- 869 Schmitz F, Königstorfer A, Südhof TC (2000) RIBEYE, a component of synaptic ribbons: a
870 protein's journey through evolution provides insight into synaptic ribbon function.
871 Neuron 28:857–872.
- 872 Schnee ME, Lawton DM, Furness DN, Benke TA, Ricci AJ (2005) Auditory hair cell-afferent fiber
873 synapses are specialized to operate at their best frequencies. Neuron 47:243–254.
- 874 Schneider CA, Rasband WS, Eliceiri KW (2012) NIH Image to ImageJ: 25 years of image analysis.
875 Nat Methods 9:671–675.
- 876 Seal RP, Akil O, Yi E, Weber CM, Grant L, Yoo J, Clause A, Kandler K, Noebels JL, Glowatzki E,
877 Lustig LR, Edwards RH (2008) Sensorineural Deafness and Seizures in Mice Lacking
878 Vesicular Glutamate Transporter 3. Neuron 57:263–275.
- 879 Sheets L, Kindt KS, Nicolson T (2012) Presynaptic CaV1.3 channels regulate synaptic ribbon size
880 and are required for synaptic maintenance in sensory hair cells. J Neurosci Off J Soc
881 Neurosci 32:17273–17286.

- 882 Sheets L, Trapani JG, Mo W, Obholzer N, Nicolson T (2011) Ribeye is required for presynaptic
883 Ca(V)1.3a channel localization and afferent innervation of sensory hair cells. *Dev Camb*
884 *Engl* 138:1309–1319.
- 885 Smith CA, Sjostrand FS (1961) Structure of the nerve endings on the external hair cells of the
886 guinea pig cochlea as studied by serial sections. *J Ultrastruct Res* 5:523–556.
- 887 Song Q, Shen P, Li X, Shi L, Liu L, Wang J, Yu Z, Stephen K, Aiken S, Yin S, Wang J (2016) Coding
888 deficits in hidden hearing loss induced by noise: the nature and impacts. *Sci Rep*
889 6:25200.
- 890 Taberner AM, Liberman MC (2005) Response properties of single auditory nerve fibers in the
891 mouse. *J Neurophysiol* 93:557–569.
- 892 Trapani JG, Nicolson T (2010) Physiological Recordings from Zebrafish Lateral-Line Hair Cells and
893 Afferent Neurons. *Methods Cell Biol* 100:219–231.
- 894 Trapani JG, Nicolson T (2011) Mechanism of spontaneous activity in afferent neurons of the
895 zebrafish lateral-line organ. *J Neurosci Off J Soc Neurosci* 31:1614–1623.
- 896 Troconis EL, Ordoobadi AJ, Sommers TF, Aziz-Bose R, Carter AR, Trapani JG (2017) Intensity-
897 dependent timing and precision of startle response latency in larval zebrafish. *J Physiol*
898 595:265–282.
- 899 Usukura J, Yamada E (1987) Ultrastructure of the synaptic ribbons in photoreceptor cells of
900 *Rana catesbeiana* revealed by freeze-etching and freeze-substitution. *Cell Tissue Res*
901 247:483–488.
- 902 Vaithianathan T, Zanazzi G, Henry D, Akmentin W, Matthews G (2013) Stabilization of
903 Spontaneous Neurotransmitter Release at Ribbon Synapses by Ribbon-Specific Subtypes
904 of Complexin. *J Neurosci* 33:8216–8226.
- 905 Wong AB, Rutherford MA, Gabrielaitis M, Pangrsic T, Göttfert F, Frank T, Michanski S, Hell S,
906 Wolf F, Wichmann C, Moser T (2014) Developmental refinement of hair cell synapses
907 tightens the coupling of Ca²⁺ influx to exocytosis. *EMBO J* 33:247–264.
- 908 Wu JS, Young ED, Glowatzki E (2016) Maturation of Spontaneous Firing Properties after Hearing
909 Onset in Rat Auditory Nerve Fibers: Spontaneous Rates, Refractoriness, and Interfiber
910 Correlations. *J Neurosci Off J Soc Neurosci* 36:10584–10597.
- 911 Zenisek D (2008) Vesicle association and exocytosis at ribbon and extra ribbon sites in retinal
912 bipolar cell presynaptic terminals. *Proc Natl Acad Sci U S A* 105:4922–4927.
- 913 Zenisek D, Horst NK, Merrifield C, Sterling P, Matthews G (2004) Visualizing synaptic ribbons in
914 the living cell. *J Neurosci Off J Soc Neurosci* 24:9752–9759.

915 Zhang QX, He XJ, Wong HC, Kindt KS (2016) Functional calcium imaging in zebrafish lateral-line
916 hair cells. *Methods Cell Biol* 133:229–252.

917 Zhao Y, Araki S, Wu J, Teramoto T, Chang Y-F, Nakano M, Abdelfattah AS, Fujiwara M, Ishihara
918 T, Nagai T, Campbell RE (2011) An Expanded Palette of Genetically Encoded Ca²⁺
919 Indicators. *Science* 333:1888–1891.

920

921

922

923

924 **FIGURE LEGENDS**

925

926 **Figure 1.** Overexpression of Ribeye b-EGFP increases ribbon size and number of tethered

927 vesicles.

928 **A,** Image of a live transgenic zebrafish expressing two copies of *ribeye b-EGFP (rib b-EGFP X 2)* in

929 hair cells at 4 dpf. Inset shows a top-down projection of a neuromast cluster of lateral-line hair

930 cells expressing Ribeye b-EGFP. **B-D** TEM images of neuromast ribbons in wild-type (WT)

931 siblings (B) and *ribeye b-EGFP* transgenic fish (C,D) at 4 dpf. **E-G,** Ectopic ribbons in hair cells

932 overexpressing of Ribeye b-EGFP. Shown are ectopic ribbons located above the nucleus. Ectopic

933 ribbons are located by the plasma membrane (E), associated with filaments (F), and near the

934 cuticular plate (G). The white arrow (E) indicates the plasma membrane of the hair cell. White

935 arrowheads (F) indicate filamentous structures in the cytosol. Black arrowheads (G) denote

936 stereocilia at the apex of the hair cell. **H-L,** Quantification of TEM images from n = 18 wild-type

937 and n = 19 *ribeye b-EGFP* ribbons from 9 and 6 neuromasts respectively. In *ribeye b-EGFP* hair

938 cells ribbon area (H) and number of tethered vesicles (J) was increased, while vesicle density (I)

939 and number of docked vesicles (K) was not altered. Compared to wild-type, vesicles were

940 slightly closer to the ribbon in *ribeye b-EGFP* hair cells (L). * P < 0.05, ** P < 0.01 using a t-test.

941 Scale bars: A = 500 μm , inset = 5 μm , B = 100 nm (same scale bar for B-G). The open circles or
942 squares (H-L) correspond to the example images shown in B-D.

943

944 **Figure 2** Overexpression of Ribeye b-EGFP increases the size of ribbons but does not increase
945 the size or number of PSDs.

946 **A,B**, Representative maximum intensity top-down (x-y) and side-view (x-z) projections of wild-
947 type (WT) (A) and transgenic *ribeye b-EGFP* (B) neuromasts with Ribeye a and Ribeye b labeling
948 ribbons (magenta) and MAGUK labeling PSDs (green) at 5 dpf. Ribeye a and b were labeled with
949 two spectrally separate fluorophores, but were both merged as magenta in the displayed

950 images. Cell nuclei labeled were with DAPI (blue). **C,D**, High-power confocal 1 μm^2 thumbnails
951 of synapses sorted by size in a representative WT (C) and a *ribeye b-EGFP* neuromast (D). A

952 number of ribbons in (D) do not have corresponding PSDs (green). **E**, Relative area (normalized
953 to wild-type median) of Ribeye puncta adjacent to PSDs, n = 192 WT and n = 132 *ribeye b-EGFP*,
954 and MAGUK puncta at ribbon-localized PSDs, n = 192 WT and n = 210 *ribeye b-EGFP* at 5 dpf. **F**,

955 Number of complete synapses per hair cell (HC), estimated by taking the total number of
956 synapses per neuromast, divided by the number of hair cells per neuromast, n = 11 wild-type
957 and n = 12 *ribeye b-EGFP* neuromasts. Each circle represents a single neuromast in an individual
958 zebrafish. Scale bars: A and B = 5 μm . **** P < 0.0001 was determined using a Mann-Whitney U
959 test. Synapse counts were not significantly different (unpaired t-test).

960

961 **Figure 3.** $\text{Ca}_v1.3a$ channel immunolabel is less clustered at enlarged ribbons.

962 **A,B**, Immunolabel of Ca_v1.3a in wild-type (WT) (A) and *ribeye b-EGFP* (B) hair cells at 5 dpf.
963 **A',B'**, Overlay of Ca_v1.3a (magenta) and the PSD label MAGUK (green) in wild-type (A') and
964 *ribeye b-EGFP* (blue) (B') hair cells. Inset on right highlights a single ribbon and corresponds to
965 boxed ROI in A' and B'. White arrowheads in B and B' indicate an enlarged ectopic ribbon with
966 no PSD, yet relatively strong Ca_v1.3a immunolabel. Ca_v1.3a immunolabeled puncta localized to
967 complete synapses, i.e. adjacent to PSDs, were examined in C and D. **C,D**, The average Ca_v1.3a
968 immunolabel intensity at sites adjacent to PSD label is greater at wild-type synapses compared
969 to *ribeye b-EGFP* synapses (C), while the total or integrated Ca_v1.3a immunolabel intensity per
970 punctum is unchanged between these groups (D), n = 282 WT and n = 125 *ribeye b-EGFP*
971 Ca_v1.3a puncta in C and D. **E**, The total amount of Ca_v1.3a immunolabel per neuromast is
972 greater in *ribeye b-EGFP* transgenics compared to wild-type. This includes Ca_v1.3a immunolabel
973 at both ectopic ribbons and at complete (PSD apposing) ribbon synapses, n = 13 WT and n = 14
974 *ribeye b-EGFP* neuromasts. **F,G**, Two example airyscan images of Ca_v1.3a and Ribeye b
975 immunolabel at wild-type (F) and *ribeye b-EGFP* ribbons (G). Right image panel in F and G is
976 Ca_v1.3a immunolabel alone, left image panel is Ca_v1.3a (magenta) and Ribeye b (green)
977 immunolabel merged. **F',G'**, Intensity profile plots represent the pixel intensity of the yellow
978 line drawn through the Ca_v1.3a immunolabel in F and G. **** P < 0.0001 using a Mann-Whitney
979 U test in C; * P = 0.01 using an unpaired t-test in E. Scale bars: B' = 5 μm (same scale bar for A-
980 B'), B inset = 1 μm, F = 1 μm (same scale bar for F-G).

981

982 **Figure 4.** Calcium currents and capacitance measurements in hair cells with enlarged ribbons.

983 **A**, Calcium currents (I_{Ca}) recorded from wild-type (WT, 7 dpf, black) or *ribeye b-EGFP* hair cells
984 (5 dpf, gray). Currents were elicited by a series of depolarizing voltage steps in 10 mV
985 increments (200 ms in duration) from the holding potential of -79 mV. For clarity, only the
986 trace at the holding potential and at the peak of I_{Ca} are shown. **B**, I-V curves of whole-cell I_{Ca} in
987 wild-type (black) and *ribeye b-EGFP* (gray) hair cells (5-8 dpf), $n = 13$ wild-type and $n = 10$ *ribeye*
988 *b-EGFP*. At the peak of I_{Ca} (-31 mV), calcium currents were significantly larger in *ribeye b-EGFP*
989 hair cells, $p > 0.05$. **C**, Changes in membrane capacitance (ΔC_m) recorded from hair cells of wild-
990 type (5 dpf, black) and *ribeye b-EGFP* transgenics (6 dpf, gray). Recordings were obtained in
991 response to 1.0-s voltage steps from the holding potential of -79 mV to near the peak of I_{Ca}
992 (-31 mV). **D**, Average ΔC_m elicited following 1.0-s depolarization step to -31 mV from hair cells
993 of both wild-type (6-8 dpf, black) and *ribeye b-EGFP* (5-8 dpf, gray) hair cells was not
994 significantly different using a t-test, $n = 6$ wild-type and $n = 7$ *ribeye b-EGFP*.

995

996 **Figure 5**. Mechanically-evoked and baseline cytosolic calcium measurements are increased in
997 hair cells with enlarged ribbons.

998 **A,B**, Live, confocal image of hair cells expressing the calcium indicator RGECO1 (A) or RGECO1
999 and Ribeye b-EGFP (B). **C**, Average mechanically-evoked calcium response of hair cells
1000 expressing RGECO1 (WT, solid blue) or RGECO1 and Ribeye b-EGFP (*ribeye b-EGFP*, dashed
1001 green) at 5-6 dpf, $n = 54$ WT and $n = 55$ *ribeye b-EGFP* hair cells. The gray bar indicates the
1002 duration of the mechanical stimulus (2.0-s). **D**, Scatterplot of the magnitude of individual hair
1003 cell responses plotted in C. **E**, Baseline RGECO calcium signals in wild-type and *ribeye b-EGFP*
1004 transgenic hair cells, $n = 74$ wild-type and $n = 96$ *ribeye b-EGFP* hair cells. A Mann-Whitney U

1005 test was used to compare calcium responses and baseline calcium signals in D and E. * $P < 0.05$,
 1006 **** $P < 0.0001$. Scale bar: A = 5 μm .

1007

1008 **Figure 6.** Ribbon-localized calcium signals are increased at enlarged ribbons.

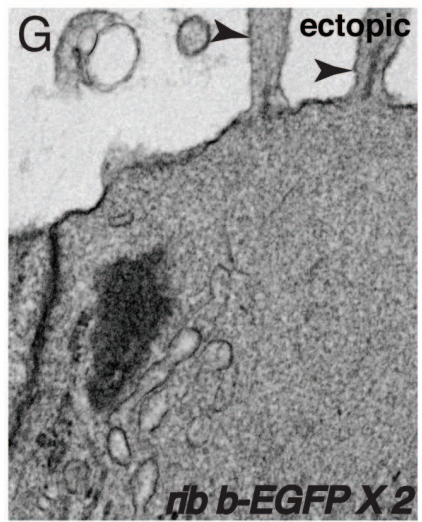
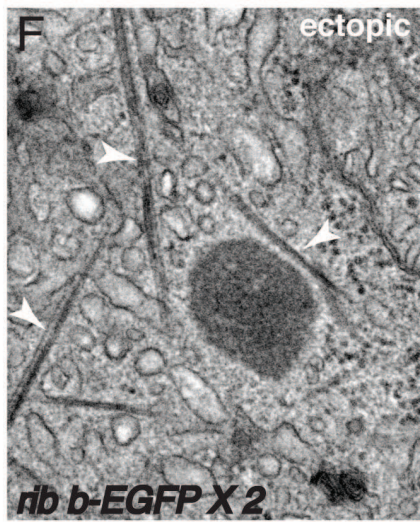
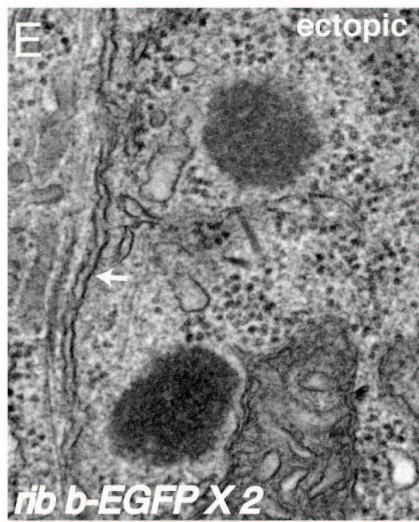
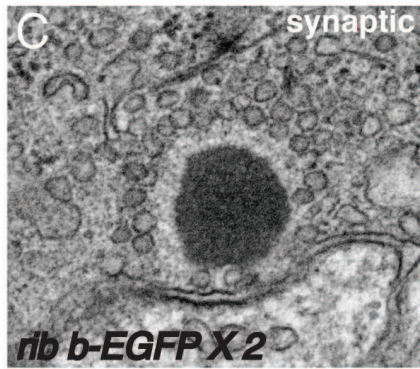
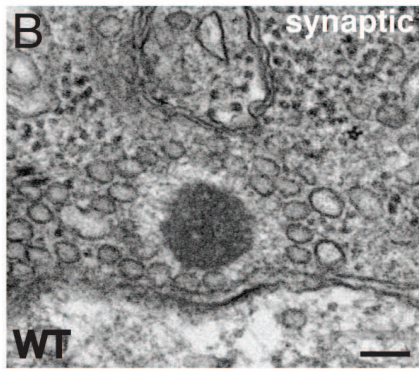
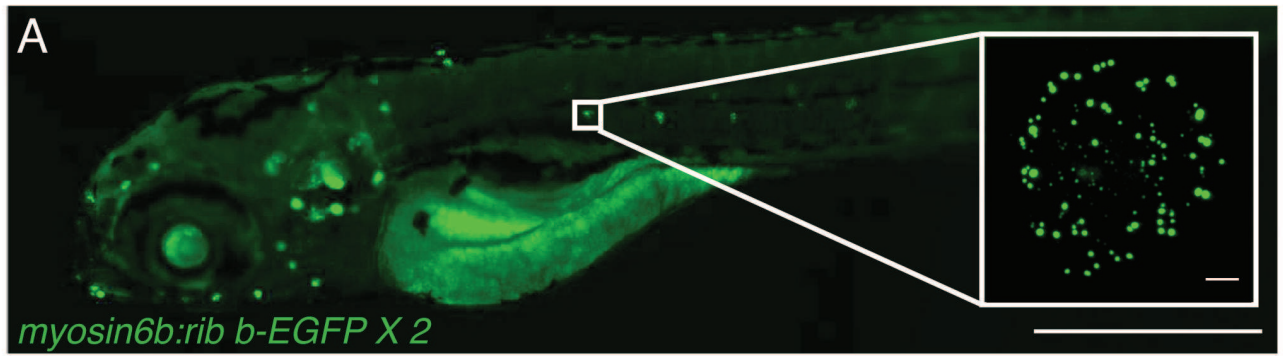
1009 **A,B,** Live images of hair cells with wild-type (WT) sized ribbons, *ribeye b-mCherry;GCaMP6s-*
 1010 *CAAX* (A) and enlarged ribbons, *ribeye a-mCherry X 2;GCaMP6s-CAAX* (B). **C,C'** Two ribbons in a
 1011 single hair cell are depicted in C. In response to a saturating, 2.0-s 5 Hz stimulus, in control hair
 1012 cells (*ribeye b-mCherry*) focal calcium hotspots are observed at individual ribbons (purple ROIs)
 1013 compared to an adjacent region (orange ROIs). Isradipine completely blocks all presynaptic
 1014 calcium signals (dashed traces in C'). **D,E** Average ribbon-localized calcium responses during a
 1015 0.5-s (D) or 0.1-s (E) stimulus at wild-type ribbons and enlarged ribbons. **E',E''** Data from E
 1016 quantified with respect to magnitude (E') and slope (E''). Measurements were performed at 4-5
 1017 dpf. In D, traces represent the average response of $n = 29$ wild-type (*ribeye b-mCherry*) and $n =$
 1018 37 enlarged (*ribeye a-mCherry*) ribbons. In E-E'', traces and data represent the average
 1019 response of $n = 27$ wild-type (*ribeye b-mCherry*) and $n = 29$ enlarged (*ribeye a-mCherry*) ribbons.
 1020 The gray bar indicates the duration of the mechanical stimulus in C', D and E. Dashed lines in D
 1021 and E represent SEM. * $P < 0.05$, using a Mann-Whitney U test. Scale bar: A = 5 μm , C = 1 μm .

1022

1023 **Figure 7.** Enlarged ribbons disrupt evoked and spontaneous afferent activity.

1024 **A,** Representative example of a 60 s recording of spontaneous action currents from wild-type
 1025 and *ribeye b-EGFP* afferent neurons. **B,** Quantification of mean spontaneous inter-spike
 1026 intervals from wild-type (WT) and *ribeye b-EGFP*, $n = 19$ wild-type and $n = 18$ *ribeye b-EGFP*

1027 neurons. **C**, Example trace from a wild-type and *ribeye b-EGFP* afferent neuron in response to a
1028 200-ms 20 Hz sine wave stimulus. Each stimulus has four cycles with positive (stimulatory)
1029 phases A-D. **D**, Average spike number for each stimulus phase (A-D) is reduced in *ribeye b-EGFP*
1030 compared to wild-type, n = 8 wild-type and n = 10 *ribeye b-EGFP* neurons. **E**, Mean time to first
1031 spike for each stimulus phase in *ribeye b-EGFP* compared to wild-type. **F**, Example sweep from
1032 the same wild-type and *ribeye b-EGFP* afferent neuron as C, in response to a 500-ms step
1033 stimulus. **G**, Average spike number per 500-ms step is the same for *ribeye b-EGFP* compared to
1034 wild-type, n = 11 neurons for wild-type and *ribeye b-EGFP*. **H**, Spike number for the first 25 ms
1035 of the 500-ms step stimulus is significantly lower in *ribeye b-EGFP* compared to wild-type. **I**,
1036 The mean first spike latency is longer in *ribeye b-EGFP* neurons compared to wild-type. * P <
1037 0.05, ** P < 0.01, *** P < 0.001 using an unpaired t-test in D, E, G, H, I. Multiple t-tests in D and
1038 E were corrected for multiple comparisons using the Holm-Sidak method. A Mann-Whitney U
1039 test was used for B.
1040
1041



● WT ■ *rib b-EGFP X 2*

